J Physiol 0.0 (2023) pp 1–21

The Journal of Physiology

Neutral sphingomyelinase regulates mechanotransduction in human engineered cardiac tissues and mouse hearts

Daniel G. P. Turner[1], Willem J. De Lange[2], Yanlong Zhu[3,4], Christopher L. Coe[5], Judith Simcox[6], Ying Ge[3,4,7], Timothy J. Kamp[1], J. Carter Ralphe[2] and Alexey V. Glukhov[1]

[1]*Department of Medicine, Cardiovascular Medicine, University of Wisconsin-Madison, Madison, WI, USA*
[2]*Department of Pediatrics, Pediatric Cardiology, University of Wisconsin-Madison, Madison, WI, USA*
[3]*Human Proteomics Program, School of Medicine and Public Health, University of Wisconsin-Madison, Madison, WI, USA*
[4]*Department of Cell and Regenerative Biology, University of Wisconsin-Madison, Madison, WI, USA*
[5]*Department of Psychology, University of Wisconsin-Madison, Madison, WI, USA*
[6]*Department of Biochemistry, University of Wisconsin-Madison, Madison, WI, USA*
[7]*Department of Chemistry, University of Wisconsin-Madison, Madison, WI, USA*

Handling Editors: Peter Kohl & Eilidh MacDonald

The peer review history is available in the Supporting Information section of this article (https://doi.org/10.1113/JP284807#support-information-section).

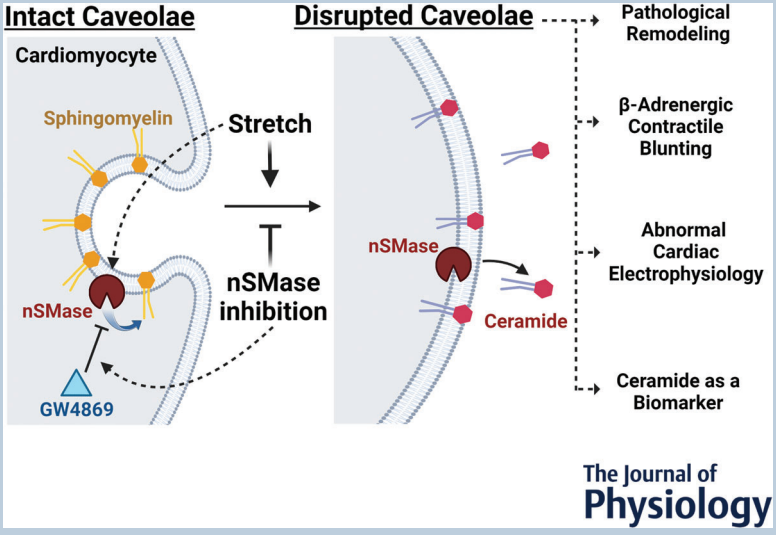

Abstract Cardiovascular disease is the leading cause of death in the USA and is known to be exacerbated by elevated mechanical stress from hypertension. Caveolae are plasma membrane structures that buffer mechanical stress but have been found to be reduced in pathological conditions associated with chronically stretched myocardium. To explore the physiological implications of the loss of caveolae, we used human engineered cardiac tissue (ECT) constructs, composed of human induced pluripotent stem cell (hiPSC)-derived cardiomyocytes and hiPSC-derived cardiac

Daniel G. P. Turner is a fifth-year graduate student studying molecular and cellular pharmacology in Dr Alexey Glukhov's laboratory at University of Wisconsin-Madison. He is anticipating the defence of his thesis focused on regulation of cardiac caveolae in early 2024. A participant in Wisconsin's prominent dairy science and industry, he previously gained experience at The Centre for Dairy Research in Madison, WI, USA. He looks forward to using his experience in disease modelling via engineered cardiac tissue to identify factors involved in various cardiac pathologies.

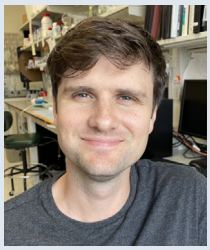

DOI: 10.1113/JP284807

fibroblasts, to develop a long-term cyclic stretch protocol that recapitulates the effects of hypertension on caveolae expression, membrane tension, and the β-adrenergic response. Leveraging this new stretch protocol, we identified neutral sphingomyelinases (nSMase) as mechanoregulated mediators of caveolae loss, ceramide production and the blunted β-adrenergic response in this human cardiac model. Specifically, in our ECT model, nSMase inhibition via GW4869 prevented stretch-induced loss of caveolae-like structures, mitigated nSMase-dependent ceramide production, and maintained the ECT contractile kinetic response to isoprenaline. These findings are correlated with a blood lipidomic analysis in middle-aged and older adults, which revealed an increase of the circulating levels of ceramides in adults with hypertension. Furthermore, we found that conduction slowing from increased pressure loading in mouse left ventricle was abolished in the context of nSMase inhibition. Collectively, these findings identify nSMase as a potent drug target for mitigating stretch-induced effects on cardiac function.

(Received 7 April 2023; accepted after revision 11 October 2023; first published online 27 October 2023)
Corresponding author A. V. Glukhov: Department of Medicine, Cardiovascular Medicine, University of Wisconsin-Madison, 8455 WIMR II, 1111 Highland Avenue, Madison, WI 53705, USA. Email: aglukhov@medicine.wisc.edu

Abstract figure legend Cardiomyocyte membranes contain caveolae that buffer mechanical stress and are known to be cardioprotective. Our study found that physical stretch activates neutral sphingomyelinase (nSMase), which converts caveolar sphingomyelin to ceramide, leading to disruption of caveolae-like structures in cardiomyocytes. We also linked stretch-induced nSMase activation to electrophysiological changes in the myocardium, including decreased ventricular conduction in mouse hearts and blunting of β-adrenergic contractile kinetics and increased ceramide production in engineered human cardiac tissue. These stretch-induced effects were prevented using GW4689, a specific nSMase inhibitor.

Key points

- We have developed a new stretch protocol for human engineered cardiac tissue that recapitulates changes in plasma membrane morphology observed in animal models of pressure/volume overload.
- Stretch of engineered cardiac tissue induces activation of neutral sphingomyelinase (nSMase), generation of ceramide, and disassembly of caveolae.
- Activation of nSMase blunts cardiac β-adrenergic contractile kinetics and mediates stretch-induced slowing of conduction and upstroke velocity.
- Circulating ceramides are increased in adults with hypertension, highlighting the clinical relevance of stretch-induced nSMase activity.

Introduction

Cardiovascular disease is the leading cause of death worldwide and is often exacerbated by underlying hypertension (Roth et al., 2020). Hypertension results in significant cardiac remodelling that leads to structural and functional changes in the heart, such as increased fibrosis and inflammation (Díez, 2007; Zhang et al., 2020), suppressed contraction, and a blunted response to sympathetic stimulation (Atkins et al., 1995). The possible mechanisms by which hypertension exacerbates cardiovascular disease are complex and reflect the myriad of pathological pathways triggered by high blood pressure, including but not limited to angiotensin II (Jiang et al., 2015), tumour necrosis factor-α (TNF-α; Chen et al., 2010) and transforming growth factor-β1 (TGF-β1; Zhang et al., 2020). In particular, the molecular mechanisms that underlie stretch-induced changes in ventricular myocardium are not completely understood.

Specialized surface membrane structures, known as caveolae, are small (50–100 nm), flask-shaped invaginations of the plasma membrane (Parton & Simons, 2007) and are composed of cholesterol, sphingomyelin and scaffolding proteins, such as cavins and caveolins (Parton et al., 2018). Caveolae provide a reserve source of 'extra' cell membrane and are implicated in cytoprotection and mechanotransduction by buffering mechanical forces

and contributing to cell volume regulation (Kozera et al., 2009; Parton & del Pozo, 2013). It has been shown that cardiac caveolae density is decreased in various animal models of cardiovascular disease associated with chronically elevated cardiomyocyte stretch, including hypertension (Egorov et al., 2019), heart failure (Wright et al., 2014) and hypertrophy (Markandeya et al., 2015). However, the mechanisms of caveolae reduction are not well understood.

Neutral sphingomyelinase (nSMase) is a membrane hydrolase enzyme that is involved in sphingolipid metabolism reactions. Activation of nSMase breaks down sphingomyelin into ceramide species of various sphingosine lengths (depending on sphingomyelin acyl-chain length) and phosphocholine (Wu et al., 2010) and can be inhibited by GW4869 (Wu et al., 2021). In skeletal muscle, caveolin-expressing membrane fractions are enriched for nSMase2 and nSMase3, whereas nSMase1 does not localize to caveolae (Moylan et al., 2014). In studies performed on non-cardiomyocyte cells, transient mechanical stress induces nSMase activity (Czarny et al., 2003), and prolonged sphingomyelinase activity reduces caveolin protein expression (Makdissy et al., 2018), suggesting nSMase-mediated caveolae disruption. Activation of nSMase produces ceramide, a potent bioactive lipid that is known to mediate fibrosis (Ji et al., 2017) and can modulate cardiac contractile function (Colligan et al., 2002). Elevated levels of ceramides are also implicated in cardiac hypertrophy and atrial fibrillation (He et al., 2012; Jensen et al., 2020).

Based on these data, we hypothesized that caveolae-localized nSMase (nSMase2 and/or nSMase3) (Moylan et al., 2014) is activated in response to stretch, produces ceramide, decreases caveolae abundance, and depresses cardiac conduction velocity that is associated with acute stretch (Pfeiffer et al., 2014). To test this hypothesis, we used a validated human engineered cardiac tissue (ECT) model consisting of human induced pluripotent stem cell (hiPSC)-derived cardiomyocytes and hiPSC-derived cardiac fibroblasts (de Lange et al., 2021). Previously, we demonstrated that these constructs respond to physiological stimuli (stretch and β-adrenergic stimulation), develop a t-tubular system, and demonstrate Ca^{2+}-handling and contractile kinetics that compare favourably with adult myocardium (de Lange et al., 2021). This *in vitro* model is free of the cardiac tissue degeneration normally observed in *ex vivo* cardiac models, thus allowing us to evaluate the effect of long-term cardiac stretch without concurrent loss of sample health.

Using our ECT cyclic stretch protocol, we show that stretch reduces abundance of caveolae-like structures, increases membrane tension and is associated with a blunted contraction kinetic response to isoprenaline. Concurrently, we show that ECT cyclic stretch increases ceramide levels and hydrogen peroxide in cell culture medium, indicating nSMase activation. Specific pharmacological inhibition of nSMase prevented downregulation of caveolae-like structures in the context of elevated mechanical stress and prevented functional changes. We complement these findings with human blood lipidomic data, implicating upregulated nSMase activity in the context of hypertension. Lastly, we demonstrate that acute cardiac stretch in mouse ventricles induces an nSMase-dependent reduction in ventricular electrical conduction and upstroke velocity.

Methods

Ethical approval

All experimental animal protocols adhered to the *Guidelines for Care and Use of Laboratory Animals* published by the National Institutes of Health (NIH; publication no. 85-23, revised 1996) and were approved by the institutional Animal Care and Use Committee (ACUC) at the University of Wisconsin-Madison (protocol ID: M005490) with steps taken to minimize pain and suffering. Healthy human hearts that went unused for organ transplant were obtained from the University of Wisconsin Organ Procurement Organization, Madison, WI, USA, as approved by the University of Wisconsin Institutional Review Board (IRB). Blood collection and testing for analysis of ceramide levels in the systemic circulation were approved by the Health Sciences IRB at the University of Wisconsin-Madison and by the IRBs at the University of California-Los Angeles and Georgetown University. We confirm that data collection and analysis involving human subjects conformed with the *Declaration of Helsinki*, except for registration in a database. All authors understand the ethical principles of *The Journal of Physiology*, and our study complies with the ethics checklist for research with animal and human subjects.

Stem cell culture

DF19-9-11T.H iPSCs, obtained from the WiCell Research Institute (RRID:CVCL_K054), were cultured in StemFlex medium (A3349401; Gibco) according to the manufacturer's protocol. Briefly, cryopreserved iPSCs were thawed, added to StemFlex medium supplemented with 5 μM Y-27632 (562822; BD Biosciences) and plated onto six-well dishes [1.5×10^5 to 3.3×10^5 cells per well (9.6 cm^2)] coated with Growth Factor Reduced Matrigel (354230; Corning). The hiPSCs were subsequently incubated at 37°C in humidified air supplemented with 5% CO_2 until they were 70–90% confluent, with medium changes every 24–48 h with StemFlex prior to passaging.

The hiPSCs were passaged every 4–6 days using Versene (15040066; Gibco) to dissociate cells according to the manufacturer's protocol, which were then resuspended in StemFlex media, and plated onto Matrigel-coated plates at a 1:6 to 1:12 split ratio.

Cardiomyocyte stem cell differentiation

Human iPSCs derived from the DF19-9-11T.H line were differentiated into cardiomyocytes (CMs) using a small molecule-directed protocol using GSK inhibition and Wnt inhibition (GiWi) as previously described (Lian et al., 2013; Zhang et al., 2012). Briefly, hiPSCs maintained on the StemFlex/Matrigel system were dissociated into single cells and seeded onto Matrigel-coated six-well plates at 2.0×10^6 cells per well in StemFlex medium. Cells were cultured for 5 days in StemFlex medium with daily medium changes. On day 0, StemFlex medium was replaced with 2.5 ml per well of RPMI (11875093) supplemented with B27 without insulin (A1895601; Gibco) supplemented with 10 μM CHIR99021 (2520691; GSK-3 inhibitor; Biogems). Precisely 24 h later (day 1), the cell culture medium was changed to 3 ml per well RPMI + B27 without insulin. On day 3, 48 h later, the medium was changed to 3 ml per well RPMI + B27 without insulin, supplemented with 5 μM IWP-2 (6866167; Biogems). Precisely 120 h later (day 5), the medium was replaced with 3 ml of RPMI + B27 without insulin. The medium was changed to RPMI + B27 complete supplement (with insulin) (17504044; Gibco) on day 7, and cells were maintained in this medium until day 15, with medium changes every 24–48 h. On day 15, cells from wells containing $\geq$50% beating cells by visual inspection were dissociated with 10× TrypLE (A1217701; Thermo Fisher Scientific) according to the manufacturer's protocol. Following resuspension in StemFlex medium, cells were replated on Synthemax (3535; Corning)-coated six-well plates at 2.0×10^6 cells per well. Roughly 48 h after replating, hiPSC-CMs were purified using lactate medium, made with RPMI 1640 with no glucose (11879020; Life Technologies), B27 supplement and 0.02% (2.66 mM) lactate (L1375; Sigma-Aldrich), for 7 days, with medium changes every 24–48 h. After selection, CMs were maintained in RPMI with B27 supplement until day 30, at which point hiPSC-CMs were dissociated for hiPSC-ECT generation (Fig. 1*A*).

Stem cell cardiac fibroblast culture

DF19-9-11T.H hiPSC-cardiac fibroblasts (CFs) were differentiated as previously described and cultured in FibroGRO-LS medium (SCMF001; Millipore Sigma) in uncoated six-well culture plates (Corning) with passaging every 4–5 days (Zhang et al., 2019). The medium was replaced every 24–48 h. Low passage numbers (<12) were used for hiPSC-ECT generation.

Generation of ECT and cyclic stretch

Day 30 DF19-9-11T.H hiPSC-CMs were inspected visually, and only wells containing $\geq$95% beating cells were dissociated with 10× TrypLE according to the manufacturer's protocol and counted using a haemocytometer. The hiPSC-CMs were subsequently resuspended in fibrin ECT medium (60.3% high-glucose DMEM; 20% F12 nutrient supplement; 1 mg/ml gentamicin; 8.75% fetal bovine serum; 6.25% horse serum; 1% HEPES; 1× non-essential amino acid cocktail; 3 mM sodium pyruvate; 0.004% (wt/vol) NaHCO3; 1 μg/ml insulin; 400 μM tranexamic acid; and 17.5 μg/ml aprotinin) and incubated for $\geq$1 h on a rotating platform at 37°C to form small and uniform clusters of viable CMs.

The DF19-9-11T.H CFs were dissociated using 1× TrypLE (12604013; Thermo Fisher Scientific) according to the manufacturer's protocol and counted using a haemocytometer. Following rotational culture, 2×10^6 hiPSC-CMs were mixed with 2×10^5 hiPSC-CFs in 200 μl fibrin ECT medium per hiPSC-ECT, a ratio similar to that previously used in the generation of three-dimensional cardiac constructs (de Lange et al., 2021; De Lange et al., 2023). To this cell mixture, 1.25 mg/ml fibrinogen and 0.5 unit of thrombin were added. This cell–matrix mixture was rapidly mixed and loaded onto a 20 mm × 3 mm cylindrical mould of FlexCell Tissue Train silicone membrane culture plate (TT4001U) and incubated in preprogrammed vacuum conditions for 60 min at 37°C supplied with air supplemented with 5% CO_2 to allow for attachment of the ECT constructs to the nylon tabs at each end of the Tissue Train well (Fig. 1*B*). Following polymerization of the fibrin matrix, ECTs were fed with ECT medium, carefully separated from the plate surface with a sterile pipette, and cultured for 30 days, with fibrin ECT medium changes every 2–3 days. The ECTs were stretched on days 53–60 (days 23–30 post-ECT generation) using a FlexCell Tissue Train silicone membrane vacuum system (Fig. 1*C*). The 7-day cyclic stretch protocol was modified from previously published protocols (Lu et al., 2021; Prosser et al., 2013) and set for 0.25 Hz and increased incrementally every 24 h by 3–4% uniaxial elongation, up to 15%. This cyclical and incremental stretch protocol was implemented because nSMase activation is transient under constant mechanical stress (Czarny et al., 2003). During the stretch protocol, all wells were fed every 48 h with ECT medium supplemented with or without GW4869. All unstretched and stretched ECTs were fed with 5 ml per well of ECT medium to maintain a proper volume of cell culture medium with concurrent sampling for downstream LC-MS/MS and H_2O_2 analyses.

GW4869 solubilization

GW4869 (501873728; Thermo Fisher Scientific), a specific nSMase inhibitor, was first diluted to 1.5 mM in dimethyl sulfoxide (DMSO), aliquoted, and stored at −80°C. Before use, aliquots were thawed at 37°C and solubilized further with 5% methanosulfonic acid at a 1:20 ratio (methanosulfonic acid:DMSO) to make a 1.43 mM GW4869 solution.

Masson's Trichrome staining and analysis

Cryo-sectioning of OCT-embedded ECT at 10 μM and Masson's Trichrome staining (catalogue no. KTMTR2) was performed by the UW-Madison Translational Research Initiatives in Pathology (TRIP) core facility. Masson's Trichrome staining images were collected using an EVOS cell imaging system at ×20 magnification. The ECT fibrotic area was evaluated in ImageJ using a custom program calculated as a percentage fibrotic area of total tissue, as discussed previously in detail (Glukhov et al., 2012).

Contraction testing of ECT

Contraction traces were measured in day 60 hiPSC-ECTs using protocols like those previously described (de Lange et al., 2021). Briefly, each hiPSC-ECT construct was transferred from the culture dish to a model 801B small intact fibre test apparatus (Aurora Scientific) in Krebs–Henseleit buffer (in mmol/L) [119 NaCl, 12 glucose, 4.6 KCl,

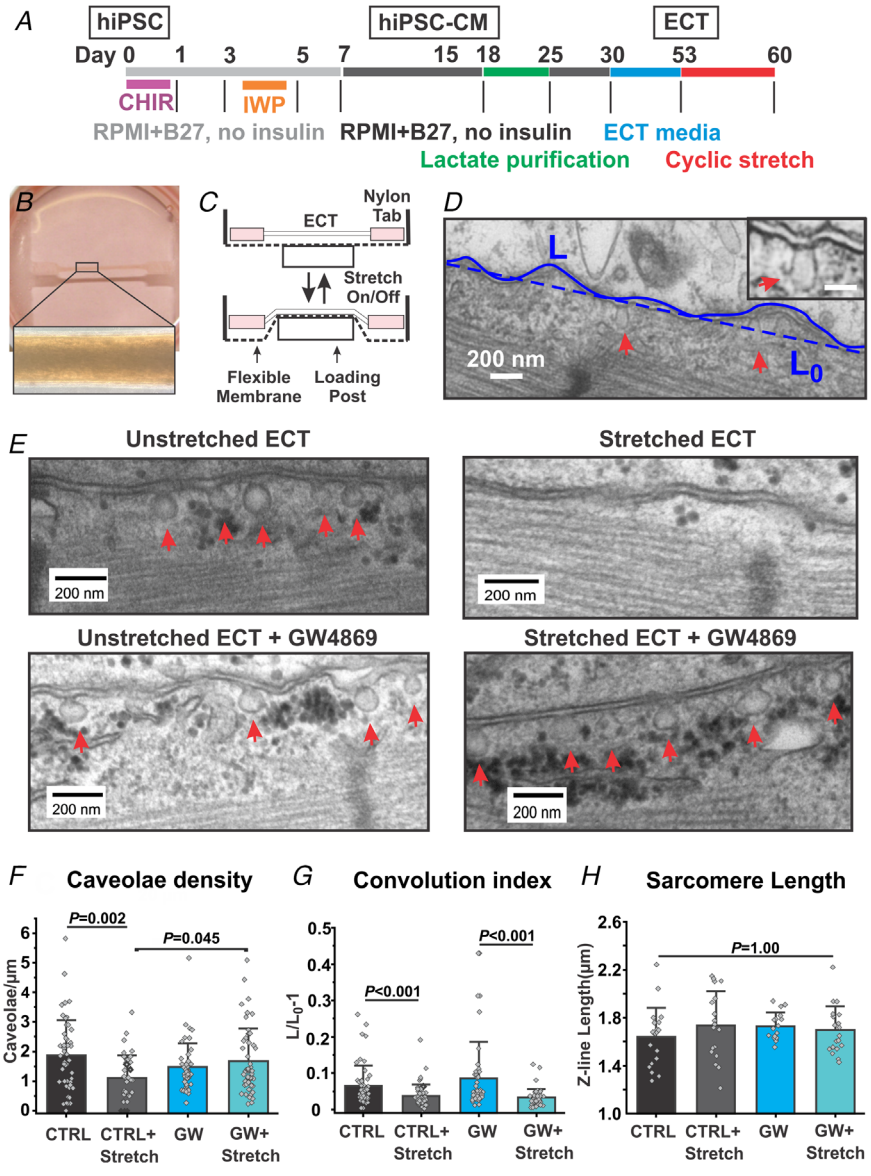

Figure 1. Cyclic stretch reduces the density of caveolae-like structures via neutral sphingomyelinase
A, time line for hiPSC-CM differentiation via GiWi protocol, hiPSC-CM purification, ECT generation and ECT cyclic stretch. *B*, representative ECT in Flexcell well and at ×10 magnification. *C*, mechanism of Flexcell stretch. *D*, representative TEM image of ECT membrane at ×40,000. *E*, representative TEM images of unstretched, stretched and GW4869-treated ECTs; red arrows indicate caveolae-like structures at ×40,000. *F*, ECT caveolae-like structure density measurements. *G*, ECT convolution index measurements. *H*, ECT sarcomere length measurements. Groups: CTRL, unstretched with vehicle; CTRL+Stretch, stretched with vehicle; GW, unstretched with GW4869; GW+Stretch, stretched with GW4869. Significance was determined by two-way ANOVA with Bonferroni's *post hoc* correction or Kruskal–Wallis tests. Means (SD) are shown; n = 4 or 5 ECTs per group (8–10 unique cardiomyocyte membrane measurements per ECT from two different sections). Abbreviations: ECT, engineered cardiac tissue; hiPSC-CM, human induced pluripotent stem cell-derived cardiomyocytes; GiWi, GSK inhibition and WnT inhibition; CHIR, CHIR99021; IWP, IWP-2; TEM, transmission electron microscopy; GW, GW4869.

25 $NaHCO_3$, 1.2 KH_2PO_4, 1.2 $MgCl_2$ and 1.8 $CaCl_2$, gassed with 95% O_2–5% CO_2 (pH 7.4)]. Day 60 hiPSC-ECT constructs were attached with sutures between a model 403A force transducer (Aurora Scientific) and a stationary arm and perfused with 37°C Krebs–Henseleit buffer at a rate of 1 ml/min, and field stimulation was initiated at 1 Hz (2.5 ms, 12.5 V). The longitudinal length of each construct was increased stepwise until maximal twitch force was achieved to establish the Frank–Starling relationship. The ECTs were allowed to equilibrate for 20 min with constant perfusion. Then, twitch force production was measured with at a 1.5 Hz pacing frequency both at baseline and after 5 min pre-incubation with 1 μM isoprenaline. Data from force measurements was analysed using IonWizard v.6.0 software (IonOptix). In each set of conditions, contraction transients of 40–60 successive contractions were collected and averaged. These data were exported to Microsoft Excel, and the kinetics of force generation and relaxation were calculated.

Transmission electron microscopy

Performed by the SMPH Electron Microscopy Facility (UW-Madison), ECTs were fixed and prepared for transmission electron microscopy (TEM) analysis while unstretched to evaluate the maximal membrane mechanical buffering capacity, in a similar manner to previous work (de Lange et al., 2021; Egorov et al., 2019). Briefly, samples were fixed in 2.5% glutaraldehyde, 2.0% paraformaldehyde buffered in 0.1 M sodium phosphate buffer for 2 h at room temperature (RT). After osmium post-fixation, dehydration and embedding, samples were sectioned on a Reichert-Jung Ultracut E ultramicrotome at 80 nm, and post-stained with uranyl acetate and lead citrate. The sectioned samples were viewed at 80 kV on a Philips CM120 transmission electron microscope at $\times$40,000 magnification. Caveolae-like structures were considered as 50–100 nm flask-shaped membrane invaginations located within 50 nm from the cell surface. Caveolae-like structures were identified as sub-sarcolemmal (no visible connection to the sarcolemma in the image plane) or visibly integrated into the sarcolemma (flask-like connection to the sarcolemma observed). To quantify the degree of membrane convolution, we defined a membrane convolution index $= (L/L_0 - 1)$, where L is the length of membrane contour, and L_0 is the length of a straight path connecting the end points of the membrane segment (Fig. 1*D*).

Mass spectrometry

Lipids were isolated from ECT medium using a modified Bligh–Dyer method (Ulmer et al., 2018) from cell culture medium (200 μl per sample). The Bligh–Dyer method was performed as previously described but using a 1:10 sample:solvent ratio during sample incubation with ice-cold methanol and chloroform (1:1) to maximize ceramide extraction. Organic samples were completely dried and reconstituted in 9:1 methanol:toluene. As previously described (Kauhanen et al., 2016), LC-MS/MS experiments were performed using a Bruker Impact II quadrupole time-of-flight (QTOF) mass spectrometer (Bruker Daltonics, Bremen, Germany) coupled to a Waters nanoACQUITY UPLC system (Waters Corporation, Milford, MA, USA) in positive ion mode. A Waters nanoEase M/Z HSS T3 column (100 Å, 1.8 μm, 300 μm $\times$ 100 mm) was used for reversed-phase separation. Mobile phase A was 10 mM ammonium acetate in water with 0.1% formic acid, and mobile phase B was 10 mM ammonium acetate in acetonitrile:2-propanol (4:3, v/v) with 0.1% formic acid (Kauhanen et al., 2016). The lipids eluted from the column were infused into the mass spectrometer using an electrospray ion (ESI) source. Lipids were identified by searching the LC-MS/MS data against the databases downloaded from MassBank of North America (MoNA) and internal databases and using Lipid Species Annotation function in MetaboScape 2022b. Detected ceramide values were adjusted with respect to the initial ECT medium protein concentration evaluated via Nanodrop.

Amplex Red peroxidase assay for ROS production

Production of H_2O_2 was measured using the supplied Ampled Red peroxidase assay kit protocol (A22188; Thermo Fisher Scientific). Briefly, a standard curve generated from the 3% H_2O_2 solution supplied in the assay kit was used to validate that H_2O_2 detection in ECT medium samples was within the linear range. Unique ECT medium samples were run in triplicate, with 50 μl of conditioned ECT medium being used for each replicate. Absorbance (560 nm) detected by a Tecan Infinite M200 plate reader was used to determine H_2O_2 production after a 30 min assay incubation at 37°C.

Assay of nSMase activity

The Amplex Red sphingomyelinase assay kit was used to quantify nSMase activity in ECT according to the manufacturer's protocol (A12220; Thermo Fisher Scientific). Briefly, ECTs were lysed and sonicated in CHAPs lysis buffer [150 mM NaCl, 50 mM Tris–HCl, 0.5% CHAPS, and 1$\times$ protease inhibitor (Bimake)]. Ten micrograms of ECT protein (run in triplicate) with and without nSMase inhibition via GW4869 (20 μM) was used during the assay. Fluorometric measurements were collected after 30 min incubation at 37°C using a Tecan

Infinite M200 plate reader with excitation/emission set for 545 nm/590 nm.

Participants for human ceramide levels

Ceramide measures were determined from randomly selected adult men and women who were participants in a survey of health and ageing among American adults, Midlife in the US (MIDUS). Initially, MIDUS began in 1995–1996 as a survey of adults recruited through random digit dialling and included individuals between 25 and 74 years of age across the 48 continental states. A second phase was initiated in 2004, when biological samples were obtained from a subset of the original participants who consented to an overnight hospital stay at one of three Clinical and Translational Research Centres, in Madison, WI or Los Angeles, CA or Washington, DC. The lipid data for this analysis were based on 520 adults between 35 and 86 years of age. A larger panel of biological and clinical measures was determined from the fasted blood samples that were obtained at ∼07.00 h. As stated previously, sample collection and testing were approved by three IRBs (Health Sciences IRB, UW-Madison, and by the IRBs at UCLA and Georgetown University). Lipidomic values were generated by mass spectrometry from frozen sera in one batch using (Complex Lipid Panel, Metabolon, Durham, NC, USA). The present analysis focuses on ceramides, but additional information on other lipids can be found in a previous publication (Berkowitz et al., 2022).

Quantitative reverse PCR

Whole ECTs and human left ventricles were snap frozen in liquid nitrogen after physiological testing and stored at −80°C. RNA was isolated as previously described (Turner et al., 2022). The hiPSC-ECTs were homogenized using TRIzol reagent (15596018; Ambion), and molecular-grade chloroform was added according to the manufacturer's instructions. After mixing, incubation and centrifugation, the aqueous phase containing RNA was collected. The RNA was purified further using the Qiagen Miniprep kit according to the manufacturer's instructions. The RNA was quantified and quality was assessed using a NanoDrop spectrophotometer (Fisher Scientific). Fifty to one hundred nanograms total RNA was reverse transcribed into first-strand complementary DNA with the iScript Reverse Transcription Supermix for RT-qPCR (170-8890; Bio-Rad), following the manufacturer's protocols. One nanogram of resulting complementary DNA was used for qPCR analysis. Taqman probes for assayed genes and appropriate controls were arrayed in MicroAmp Optical 96-well Reaction Plates (4483485; Applied Biosystems), and the PCR was performed using the TaqMan Gene Expression Master Mix (4369016; Applied Biosystems). Real-time monitoring of TaqMan fluorescence was performed on the Bio-Rad RT-qPCR system CFX96. An initial activation step of 2 min at 50°C and 10 min at 95°C was followed by 40 cycles of 15 s of denaturation at 95°C and 60 s of annealing/extension at 60°C. Data were analysed in Excel, using a ΔΔCT method, as previously described (Turner et al., 2022), with *GAPDH* used as a housekeeping control gene. TaqMan assay IDs used were as follows: *GAPDH* (Hs02786624_g1), *ACTA2* (Hs05005341_m1), *COL3A1* (Hs00943809_m1), *COL1A2* (Hs01028956_m1), *TIMP3* (Hs00165949_m1), *MMP2* (Hs01548727_m1), *TGF-β1* (Hs00998133_m1), *TNF-α* (Hs00174128_m1), *IL-6* (Hs00174131_m1), *SMPD4* (Hs04187047_g1) and *SMPD3* (Hs00920354_m1). All TaqMan assays were obtained from Applied Biosystems unless indicated otherwise.

Isolated mouse heart studies

Adult (5- to 7-month-old) male and female C57BL/6 mice (RRID:MGI:2159769; $n = 8$) were used in the study. Hearts were isolated and Langendorff perfused as described previously (Glukhov et al., 2010). Mice were heparinized and anaesthetized, and the heart was removed and placed in oxygenated (95% O_2–5% CO_2), constant-temperature (37°C) modified Tyrode solution of the following composition (in mmol/L): 128.2 NaCl, 4.7 KCl, 1.19 NaH_2PO_4, 1.05 $MgCl_2$, 1.3 $CaCl_2$, 20.0 $NaHCO_3$ and 11.1 glucose (pH = 7.35 ± 0.05). After cannulation, the heart was superfused and retrogradely perfused with warmed (37°C) Tyrode solution under a constant aortic pressure of 60 mmHg. The heart was paced at the lateral left ventricular midwall with a silver bipolar electrode coated with Teflon except at the tip. As previously described (Pfeiffer et al., 2014), once isolated and connected to Langendorff perfusion apparatus, a fluid-filled length of polyethylene tubing fitted onto a 20-gauge luer adapter was inserted into the left ventricular cavity via the pulmonary vein and mitral valve. A tie was secured around the opening of the pulmonary vein. The left ventricular cavity tube was connected to a reservoir of warmed and oxygenated perfusate, and left ventricular pressure was controlled by the height of the reservoir relative to the heart.

Optical mapping of whole mouse hearts

As previously described (Glukhov et al., 2010), coronary-perfused hearts were stained by perfusion with voltage-sensitive dye (RH-237, S1109; Thermo Fisher Scientific; 5 μl of 1 mg/ml DMSO, in Tyrode solution) for 10 min. Excitation light (530 nm/540 nm) was generated by a 150 W halogen lamp with an

excitation filter (530–540 nm) from a constant-current, low-noise power supply (MHAB-150W; Moritex USA, CA, USA). The emitted light >660 nm was filtered by a long-pass filter (>660 nm; Thorlabs, NJ, USA) for the action potential signal. The fluorescent light emitted from the preparation was long-pass filtered (>660 nm) using an edge pass filter (Thorlabs) before reaching the camera. Emitted light was directed towards a MiCAM Ultima-L CMOS camera (SciMedia, CA, USA) with high spatial (100 × 100 pixels, 60 ± 10 μm per pixel) and temporal (2000 frames/s) resolution. The acquired fluorescence signal was digitized, amplified and visualized using custom software (SciMedia, CA, USA). A customized Matlab-based computer program was used to analyse optical signals. The maximal upstroke derivative (dV/dt_{max}) was calculated for each action potential using the normalized optical signal and its derivatives. Activation maps were constructed during constant 8 Hz electrical pacing from activation times, which were determined from the dV/dt_{max}.

Statistical analysis

For assessing the effect of cyclic stretch on ECT plasma membrane morphology, fibrosis, β-adrenergic stimulation and stretch-conditioned medium, *P*-values were calculated using two-way ANOVA with Bonferroni's *post hoc* multiple comparisons test to test for interactions when comparing multiple groups in cases where the data displayed a normal distribution. If the Shapiro–Wilk test revealed that the data did not have a normal distribution, Kruskal–Wallis ANOVA was used. Statistical significances between normotensive and hypertensive MIDUS participant ceramide data were determined via Welch's Student's *t* tests. Correlations were evaluated using linear regression, with significance calculated using an *F*-test. Statistical analyses were performed in Origin or GraphPad Prism software, and *P*-values of $\leq$0.05 were considered statistically significant. All confidence intervals (CI) are 95%.

Results

Chronic cyclic stretch alters ECT plasma membrane morphology via nSMase

To determine stretch-induced changes in cardiac myocytes, ECTs were subjected to cyclic stretch for 7 days using a previously published protocol (Lu et al., 2021) for cyclical and incremental stretch modified for elevated mechanical stress. Adjusting for human myocardium, we stretched our ECT at 0.25 Hz and increased incrementally every 24 h by 3–4% elongation, up to 15% length increase over unstretched length, based on Prosser et al. (2013). TEM analysis revealed that cyclic stretch reduced the abundance of caveolae-like structures by 41%, from 1.87 caveolae/μM (CI 1.53–2.20) in unstretched ECTs to 1.11 caveolae/μM (CI 0.86–1.35) in stretched ECT ($P = 0.002$, two-way ANOVA with Bonferroni's *post hoc* test; Fig. 1*F*).

Furthermore, nSMase inhibition via GW4869 (20 μM) applied during the 7-day stretch protocol prevented the effects of cyclic stretch on caveolae-like structure reduction with a 51% increase in stretched ECT treated with GW4869 (1.68 caveolae/μM, CI 1.36–1.98) compared with untreated stretched ECT (1.11 caveolae/μM, CI 0.86–1.35; $P = 0.045$, two-way ANOVA with Bonferroni's *post hoc* test). In stretched ECTs, the reduction in caveolae-like structures was accompanied by a 43% decrease in membrane convolution (0.037, CI 0.028–0.046) compared with unstretched ECTs (0.065, CI 0.049–0.081), indicating increased membrane tension ($P < 0.001$, Kruskal–Wallis test; Fig. 1*G*) (Egorov et al., 2019; Wei et al., 2017). As anticipated, incubation with GW4869 did not prevent a significant reduction in membrane convolution ($P < 0.001$, Kruskal–Wallis test) in stretched ECT (0.033, CI 0.027–0.040) *vs.* unstretched ECT (0.086, CI 0.057–0.115), indicating that despite increased membrane tension, nSMase inhibition still prevents stretch-induced reductions in caveolae-like structures.

Cyclic stretch increases ceramide and reactive oxygen species in ECT cell culture medium

Studies have shown that inflammatory cardiovascular conditions increase ceramide levels in the heart (He et al., 2012) and blood (Jensen et al., 2020); however, the contribution of nSMase to these increased ceramides is unknown. To explore the potential mechano-activation of nSMase and its role in mediating cardiovascular pathology, we used LC-MS/MS on ECT cell culture medium to determine nSMase activity. The LC-MS/MS analysis found that cell culture medium collected from cyclically stretched ECT medium had a 38% increase of short-chain ceramides (1.00, CI 0.86–1.14) compared with unstretched ECT medium (1.38, CI 1.16–1.60; Fig. 2*A*; $P = 0.004$, two-way ANOVA with Bonferroni's *post hoc* test), with no change in long-chain ceramides (Fig. 2*B*; $P = 0.560$, two-way ANOVA with Bonferroni's *post hoc* test).

GW4869 treatment prevented short-chain ceramide production between unstretched (1.16, CI 1.06–1.27) and stretched ECT (1.21, CI 1.04–1.37; $P = 1.00$, two-way ANOVA with Bonferroni's *post hoc* test), indicating nSMase as a key mediator of stretch-induced short-chain ceramide production in cardiac tissue. Importantly, we demonstrated that GW4869-treated ECT lysate had nSMase activity (2553, CI 1886–3320) reduced by 32.5% compared with untreated ECT lysate (3644, CI 2680–4609;

$P = 0.005$, Student's paired t test), suggesting that GW4869 is effective in cardiac tissue (Fig. 2*E*).

Furthermore, our data indicated that GW4869 effectively inhibits nSMase3, because RT-qPCR detected *SMPD4* (encoding nSMase3) but not *SMPD3* (encoding nSMase2) mRNA in ECT or adult human left ventricle, and that *SMPD4* is the predominant membrane-associated nSMase in mouse left ventricle (Fig. 2*F*). RT-qPCR analysis also revealed no changes in *SMPD4* mRNA, when comparing unstretched (0.068, CI 0.042–0.093) and stretched ECT (0.040, CI 0.024–0.11; $P = 0.846$, two-way ANOVA with *post hoc* Bonferroni correction; Fig. 2*D*). Protein expression of nSMase3 was unchanged between unstretched and stretched ECT (data not shown). This suggests that nSMase3, not nSMase2, in our ECT is the main nSMase mediator of stretch-induced changes in caveolae-like structures and ceramide production.

Overall, these findings support our hypothesis of stretch-induced nSMase activation. Other possible stretch-induced pathogenic factors in myocardium are reactive oxygen species (ROS) (Gao et al., 2021), which have also been shown to play a role in the activation of nSMase via NADPH oxidase (NOX) (Hernandez et al., 2000). Although we found that cyclic stretch increased ROS production in ECT medium, from 0.33 (CI 0.32–0.34) in unstretched medium to 0.36 (CI 0.35–0.37; $P < 0.001$, two-way ANOVA with *post hoc* Bonferroni correction) in stretched medium, it was unaffected by nSMase inhibition, with no significant difference between stretch (0.36, CI 0.35–0.37) and GW4869+Stretch (0.37, CI 0.35–0.39; $P = 1.00$, two-way ANOVA with *post hoc* Bonferroni correction; Fig. 2*C*). This suggests that nSMase is downstream of NOX2 during mechanotransduction, but additional studies are required to determine whether nSMase mechano-activation is NOX2 dependent.

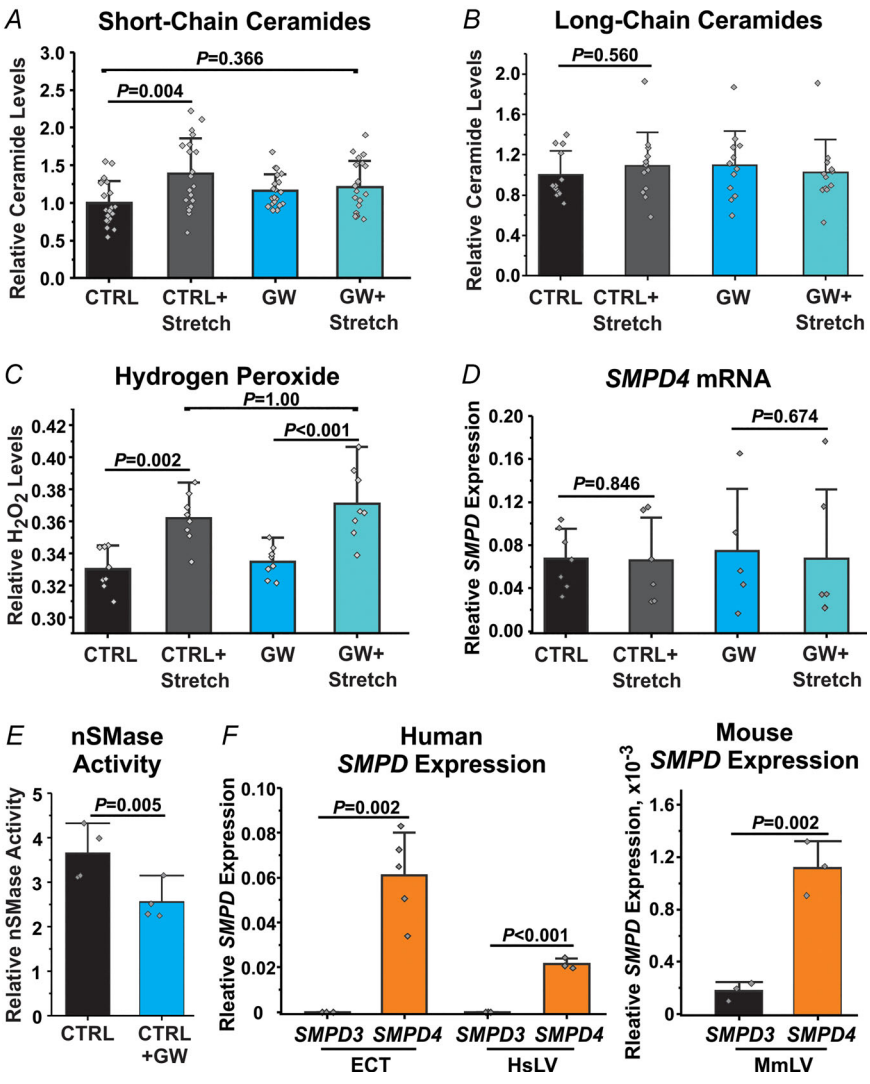

Figure 2. Cyclic stretch induces production of ceramide via neutral sphingomyelinase 3 and reactive oxygen species (neutral sphingomyelinase independent)
Relative levels of short-chain ceramides (*A*; acyl side chain <26) and long-chain ceramides (*B*; acyl side chain >26) from ECT cell culture medium after 4 h of cyclic stretch. *C*, relative hydrogen peroxide levels of ECT after 1 h of cyclic stretch. *D*, *SMPD4* mRNA expression relative to *GAPDH* in ECT. *E*, ECT nSMase activity with and without 20 μM GW4869. *F*, *SMPD* mRNA expression relative to *GAPDH* in ECT and human left ventricle (HsLV, left) and mouse left ventricle (MmLV, right). Significance was determined via two-way ANOVA with Bonferroni's *post hoc* correction or Student's *t* test. Means (SD) are shown; $n = 4$ ECT medium per group; $n = 3$–7 ECT per group for gene expression experiments; $n = 3$ mice. Abbreviations: ECT, engineered cardiac tissue; nSMase, neutral sphingomyelinase; GW, GW4869; *SMPD*, sphingomyelin phosphodiesterase.

Inhibition of nSMase prevents chronic cyclic stretch effects on ECT contraction kinetics

It has been shown that caveolae play a crucial role in the regulation of cAMP signalling and the cardiomyocyte response to sympathetic stimulation (Calaghan & White, 2006; Wright et al., 2014). Loss of caveolae has been linked to an abnormal response to β-adrenergic receptor stimulation (Rybin et al., 2003) and reported for heart failure patients (Böhm et al., 1988). To determine whether the observed stretch-induced reductions in caveolae-like structures modulate ECT response to sympathetic stimulation, we performed contraction testing on unstretched and stretched ECTs. Analysis of ECT twitch amplitude and kinetics before and after treatment with the β-adrenergic receptor agonist isoprenaline (1 μM) revealed significant changes in ECT response, as demonstrated in Fig. 3.

Initially, we found that stretched ECT exhibited a significantly blunted response to isoprenaline (P = 0.024, Kruskal–Wallis test), as indicated by an 11% decrease of the total contraction time to 100% peak force (CT100) in unstretched ECT (−1.13, CI −2.01 to −0.23) compared with stretched ECT (−0.12, CI −0.53 to 0.29; Fig. 3*B*). This blunted response was prevented by GW4869 treatment, suggesting an nSMase- and caveolae-mediated role. In addition, no significant changes in isoprenaline response were observed in the time to 50 and 90% relaxation (RT50 and RT90, respectively) between unstretched (−1.34, CI −2.65 to −0.028 and −1.55, CI −2.91 to −0.18, respectively) and stretched ECT (−0.60, CI −1.11 to −0.1 and −0.58, CI −1.06 to −0.1; P = 0.735 and 0.436, respectively, two-way ANOVA with Bonferroni's *post hoc* correction; Fig. 3*C* and *D*), suggesting that the stretch protocol has a larger effect on excitation–contraction coupling rather than

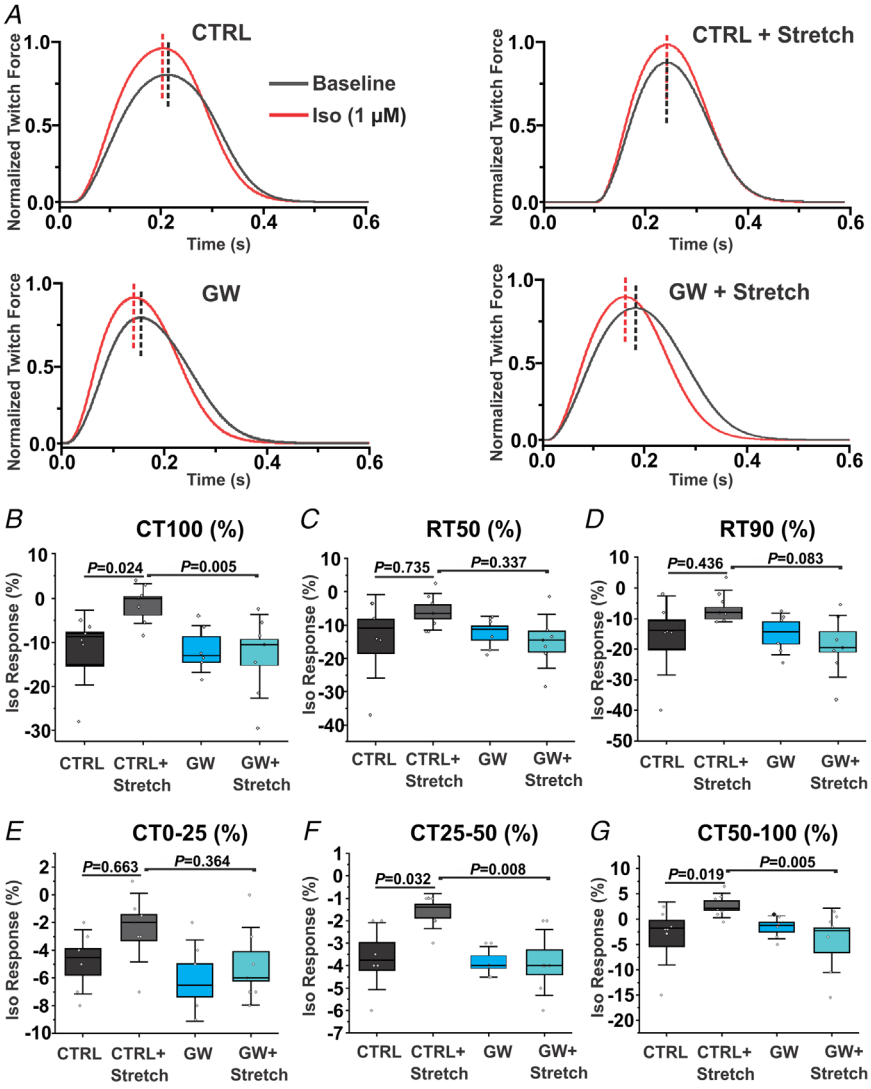

Figure 3. Cyclic stretch blunts engineered cardiac tissue β-adrenergic contractile kinetics in a neutral sphingomyelinase-dependent manner
A, representative ECT contraction traces before and after 1 μM isoprenaline paced at 1.5 Hz; vertical dotted lines indicate maximal contraction. B–G, isoprenaline-induced change in ECT paced at 1.5 Hz in time to 100% contraction (CT100; *B*), time to 50% relaxation (RT50; *C*), time to 90% relaxation (RT90; *D*), time for 0 to 25% contraction (CT0-25; *E*), time for 25 to 50% contraction (CT25-50; *F*) and time for 50 to 100% contraction (CT50-100; *G*). Groups: CTRL, unstretched with vehicle; CTRL+Stretch, stretched with vehicle; GW, unstretched with GW4869; GW+Stretch, stretched with GW4869. Significance was determined either with Kruskal–Wallis tests or with two-way ANOVA with Bonferroni's *post hoc* correction. Means (SD) are shown; n = 6 or 7 ECTs per group. Abbreviations: ECT, engineered cardiac tissue; Iso, isoprenaline; GW, GW4869.

Ca^{2+} reuptake. Looking further, we found that stretched ECT have a 2.0 and 5.5% blunted kinetic response to isoprenaline with respect to contraction times 25 to 50% and 50 to 100% (CT25-50 and CT50-100, respectively; $P = 0.032$ and 0.019, respectively, Kruskal–Wallis test; Fig. 3*F* and *G*) but not 0 to 25% (CT0-25; $P = 0.663$, Kruskal–Wallis test; Fig. 3*E*). For CT0-25, CT25-50 and CT50-100, unstretched mean ECT relative responses to isoprenaline were −0.48 (CI −0.72 to −0.24), −0.36 (CI −0.51 to −0.20) and −0.28 (CI −0.94 to 0.37), respectively, and stretched ECT responses were −0.23 (CI −0.46 to 0.00), −0.16 (CI −0.23 to −0.08) and 0.27 (CI 0.049–0.49), respectively.

Stretch and nSMase inhibition had no effect on absolute twitch forces, ECT baseline contraction kinetics or arrhythmogenesis (data not shown) in response to isoprenaline ($P = 1.00$, two-way ANOVA with Bonferroni's *post hoc* correction; Fig. 4). In addition, stretch and GW4869 had no significant effect on sarcomere length ($P = 1.00$, two-way ANOVA with Bonferroni's *post hoc* correction; Fig. 1*H*), further suggesting the effects of caveolae disassembly on ECT contraction, rather than changes to sarcomere ultrastructure. These findings indicate that our cyclic stretch protocol not only alters ECT plasma membrane morphology but also has a significant caveolae- and nSMase-mediated effect on ECT β-adrenergic response.

RT-qPCR of unstretched and stretched ECTs of fibrotic and inflammatory pathways

Given that both chronically elevated stretch (Díez, 2007) and ceramide (Ji et al., 2017) have been linked to the activation of fibrogenesis and inflammatory-associated pathways, we used RT-qPCR to evaluate the effect of stretch and nSMase inhibition on our ECTs. We found that stretch and GW4869 had a limited effect on fibrosis. We observed a significant decrease in fibrotic area only between stretched (9.11% fibrosis, CI 7.72–10.50) and GW4869+Stretch ECT (6.52% fibrosis, CI 5.52–7.52; $P = 0.017$, two-way ANOVA with Bonferroni's *post hoc* correction), but no statistically significant change in non-stretched and stretched ECT ($P = 0.609$, two-way ANOVA with Bonferroni's *post hoc* correction), determined by Masson's Trichrome staining (Fig. 5*A* and *B*). With regard to mRNA expressions, we observed a significant increase only in *ACTA2* between unstretched (1.00, CI 0.66–1.23) and stretched ECT treated with GW4869 (2.16, CI 1.49–2.83; $P = 0.005$, two-way ANOVA with Bonferroni's *post hoc* correction) and unstretched (1.02, CI 0.75–1.29) and stretched ECT both treated with GW4869 ($P = 0.006$, two-way ANOVA with Bonferroni's *post hoc* correction; Fig. 5*C*). In contrast, qPCR analysis revealed that stretch did not have a significant effect between unstretched and

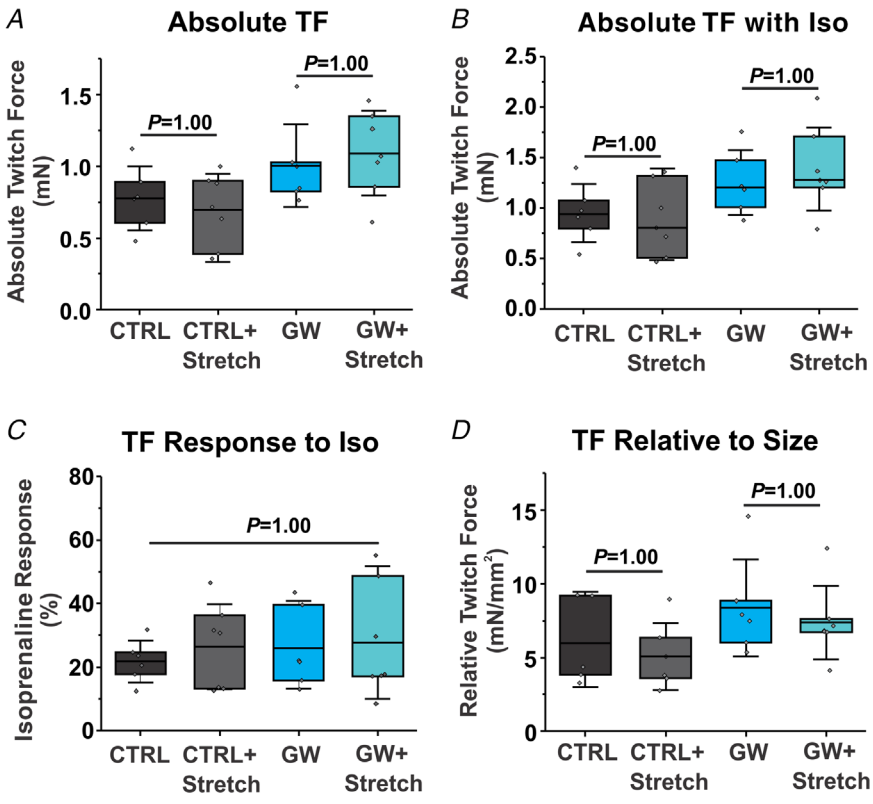

Figure 4. Cyclic stretch and GW4869 have no effect on engineered cardiac tissue twitch force
A and *B*, absolute ECT twitch force at baseline (*A*) and after 1 μM isoprenaline (*B*). *C* and *D*, ECT twitch force response to 1 μM isoprenaline (*C*) and relative to ECT size (*D*). Groups: CTRL, unstretched with vehicle; CTRL+Stretch, stretched with vehicle; GW, unstretched with GW4869, GW+Stretch, stretched with GW4869. Significance was determined via two-way ANOVA with Bonferroni's *post hoc* correction. Means (SD) are shown; n = 5–7 ECTs per group. Abbreviations: ECT, engineered cardiac tissue; GW, GW4869.

stretched ECT for other fibrosis-related mRNAs, such as *COL3A1* (P = 0.100, Kruskal–Wallis test), *COL1A2* (P = 0.438, Kruskal–Wallis test), *TIMP3* (P = 0.474, Kruskal–Wallis test), *MMP2* (P = 1.00, two-way ANOVA with Bonferroni's *post hoc* correction) and *TGF-β1* (P = 0.603, Kruskal–Wallis test; Fig. 5*D*–*H*). Lastly, mRNAs for the inflammatory cytokines *TNF-α* and *IL-6* were not detected (data not shown).

Effect of hypertension on human circulating ceramide levels in humans

Publicly available blood lipidomic values from the MIDUS survey of health in the USA were evaluated to determine whether hypertension was correlated with ceramide levels among middle-aged and older American adults (https://www.midus.wisc.edu/). Serum

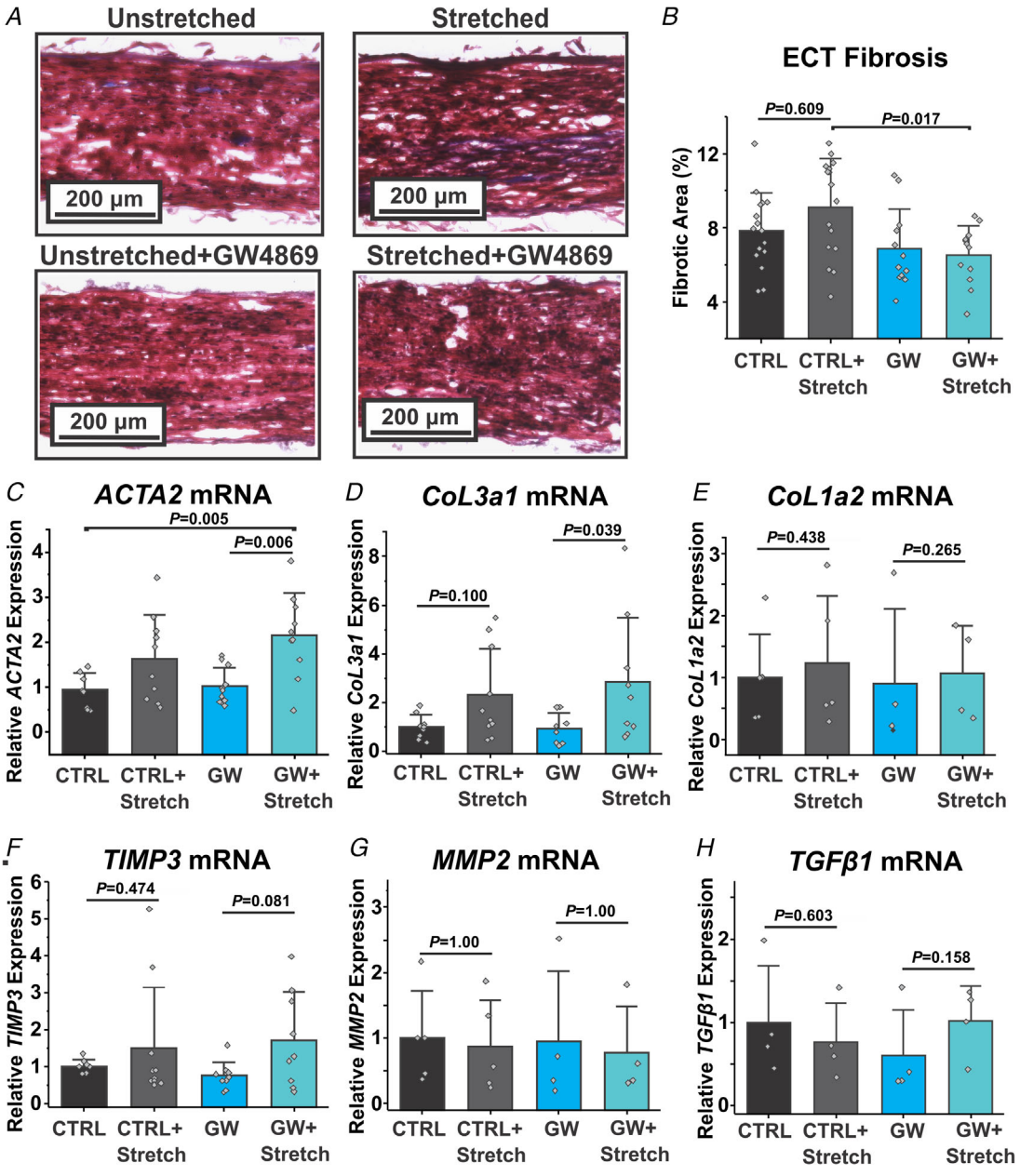

Figure 5. Stretch has a limited effect on engineered cardiac tissue fibrosis
A and *B*, representative Masson's Trichrome staining ECT images (*A*) and quantification of fibrotic area percentage (*B*); n = 3 or 4 ECTs per group, with four measurements from two sections per ECT. *C*–*H*, RT-qPCR analysis of *ACTA2* (*C*), *COL3A1* (*D*), *COL1A2* (*E*), *TIMP3* (*F*), *MMP2* (*G*) and *TGF-β1* (*H*), relative to *GAPDH*. n = 4–10 ECTs per group. Groups: CTRL, unstretched with vehicle; CTRL+Stretch, stretched with vehicle; GW, unstretched with GW4869, GW+Stretch, stretched with GW4869. Significance was determined via two-way ANOVA with Bonferroni's *post hoc* test or Kruskal–Wallis test. Error bars are SD. Abbreviations: ECT, engineered cardiac tissue; GW, GW4869.

lipidomic data were acquired from ∼120 hypertensive and ∼420 normotensive adult participants. To identify significant differences in distinct subgroups, individuals were categorized by sex and age (>50 or <50 years of age). We found that ceramide 18:0 was increased by 22 and 17% in hypertensive males (0.111 μM, CI 0.096–0.126 *vs.* 0.090 μM, CI 0.083–0.098) and females (0.113 μM, CI 0.104 to 0.121 *vs.* 0.0904 μM, CI 0.088–0.100) >50 years of age ($P = 0.013$ and $P < 0.001$, respectively, Welch's *t* test), respectively, and ceramide 24:1 was increased by 19% in men >50 years of age (0.76 μM, CI 0.65–0.87 *vs.* 0.64 μM, CI 0.60–0.68; $P = 0.039$, Welch's *t* test; Fig. 6). In men <50 years of age, no ceramides were elevated in hypertensive individuals, whereas ceramides 16:0 and 20:0 were higher by 8% (0.287 μM, CI 0.270–0.304 *vs.* 0.266 μM, CI 0.256–0.276) and 16% (0.085 μM, CI 0.076–0.094 *vs.* 0.073 μM, CI 0.067–0.079), respectively, in hypertensive women <50 years of age ($P = 0.040$ and 0.028, respectively, Welch's *t* test; Fig. 7*A*). Interestingly, ceramides 16:0, 24:0 and 24:1 were elevated by 6% (0.282 μM, CI 0.269–0.295 *vs.* 0.266 μM, CI 0.256–0.276), 14% (2.17 μM, CI 2.03–2.30 *vs.* 1.91 μM, CI 1.81–2.01) and 10% (0.65 μM, CI 0.60 to 0.70 *vs.* 0.59 μM, CI 0.55–0.62), respectively, ($P = 0.050$, 0.003 and 0.050, respectively, Welch's *t* test) in normotensive men <50 years of age compared with normotensive women <50 years of age (Fig. 7*B*). These findings suggest that there is an increase in nSMase activity in hypertensive individuals; however, studies with inhibitors of other ceramide producers, such as ceramide synthases (Rodriguez-Cuenca et al., 2015) and acid sphingomyelinase (Pavoine & Pecker, 2009), are needed to confirm this interpretation.

Acute mechanically mediated activation of nSMase

To provide further support for our ECT findings and demonstrate that nSMase is activated during stretch, we applied high-resolution fluorescent optical mapping of electrical activity during acute ventricular pressure loading on wild-type mice (Fig. 8). Using this model, Pfeiffer et al. (2014) previously demonstrated that acute myocardial stretch induces conduction velocity slowing. We hypothesized that nSMase mediates this stretch-induced conduction slowing, which is supported by the findings of Shi et al. (2020) that nSMase inhibition prevents shear stress-induced membrane depolarization in vascular tissue, which could affect sodium channel activation and subsequent conduction velocity slowing.

Acute stretch (10 min) via pressure loading of mouse left ventricle resulted in a 29 and 31% decrease in longitudinal (0.71, CI 0.67–0.76 *vs.* 1.00, CI 0.81–1.18) and transversal (0.69, CI 0.51–0.88 *vs.* 1.00, CI 0.63–1.38) conduction velocity, respectively ($P < 0.001$, two-way

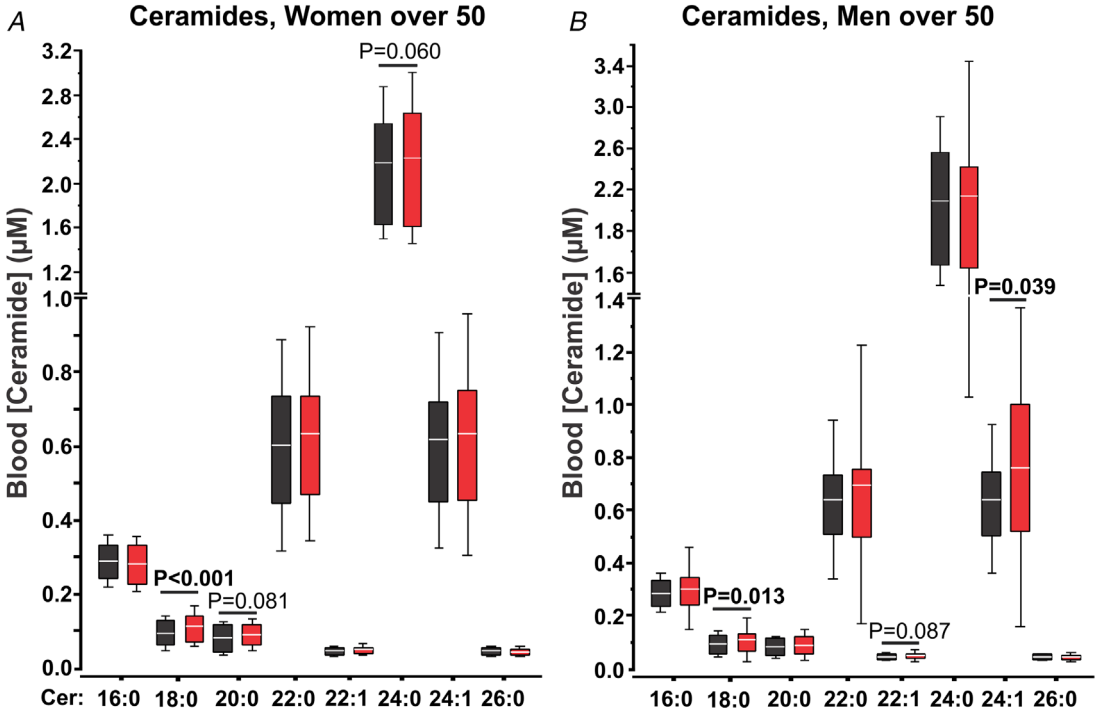

Figure 6. Blood ceramide levels in American adults >50 years of age, with or without hypertension
Absolute ceramide concentrations (micromolar) of women (*A*) and men (*B*) >50 years of age. Significance was determined via Welch's *t* test. Means (SD) are shown. Black or red bars indicate normo- or hypertensive groups, respectively; *n* = 60–200 human blood samples.

ANOVA with Bonferroni's *post hoc* correction; Fig. 9*A* and *B*), normalized to baseline, with no change in conduction anisotropy in control (2.04, CI 0.91–3.17 at baseline *vs.* 2.1, CI 0.99–3.21 during loading, $P = 1.00$, two-way ANOVA with Bonferroni's *post hoc* correction) and GW4869-treated ventricles (2.39, CI 1.92–2.86 at baseline *vs.* 2.39, CI 2.09–2.69 during loading, $P = 1.00$, two-way ANOVA with Bonferroni's *post hoc* correction). Upon unloading (20 min), both conduction velocities returned to baseline levels. More importantly, pretreatment of mouse hearts with the nSMase inhibitor GW4869 (5 μM) completely prevented the effect of stretch-induced conduction velocity slowing ($P < 0.001$, two-way ANOVA with Bonferroni's *post hoc* correction). Acute stretch also resulted in a reversable decrease in maximal upstroke velocity (dV/dt_{max}; Fig. 9*C*), which was prevented by pretreatment with GW4869 (9.63, CI 8.12–11.12 *vs.* 12.23, CI 10.90–13.55; $P = 0.020$, two-way ANOVA with Bonferroni's *post hoc* correction). Furthermore, we observed a small but significant correlation between dV/dt_{max} and conduction velocity ($r^2 = 0.38$, $P = 0.033$, *F*-test; Fig. 9*D*), which might suggest that the stretch-induced diminished activity of Na^+ channels is a contributor to the observed conduction slowing. These findings identify nSMase as a key mediator of stretch-induced cardiac conduction slowing that can be observed during acute cardiac pressure overload.

Discussion

Although the cardioprotective effects of caveolae are well documented (Kozera et al., 2009; Markandeya et al., 2015; Patel et al., 2007; Turner et al., 2022), it is unclear how caveolae loss occurs during cardiac pathologies accompanied by chronically elevated myocardial stretch. This gap in knowledge is exacerbated by a lack of cardiac models that can distinguish the mechanisms of mechanical stress over long periods of time from other factors that might also contribute to caveolae remodelling. Using hiPSC-based ECT constructs, we developed an *in vitro* protocol for modelling stretch-induced changes in cardiac structure and function, including a reduction in caveolae-like structures. We showed that the effects of cyclic stretch on ECT plasma membrane organization recapitulates the effects observed in mice after transaortic constriction (Markandeya et al., 2015; Wei et al., 2017). Several important features support the validity of the human ECT model to advance our understanding of caveolae biology. First, absolute caveolae density is similar between mice and the human ECT model. Second, both mice with transaortic constriction and cyclic stretch of ECT reduce the plasma membrane convolution index to a similar degree, with a comparable reduction in caveolae abundance. These data suggest that our ECT can model some of the effects of increased mechanical stress that might occur in an elevated mechanical

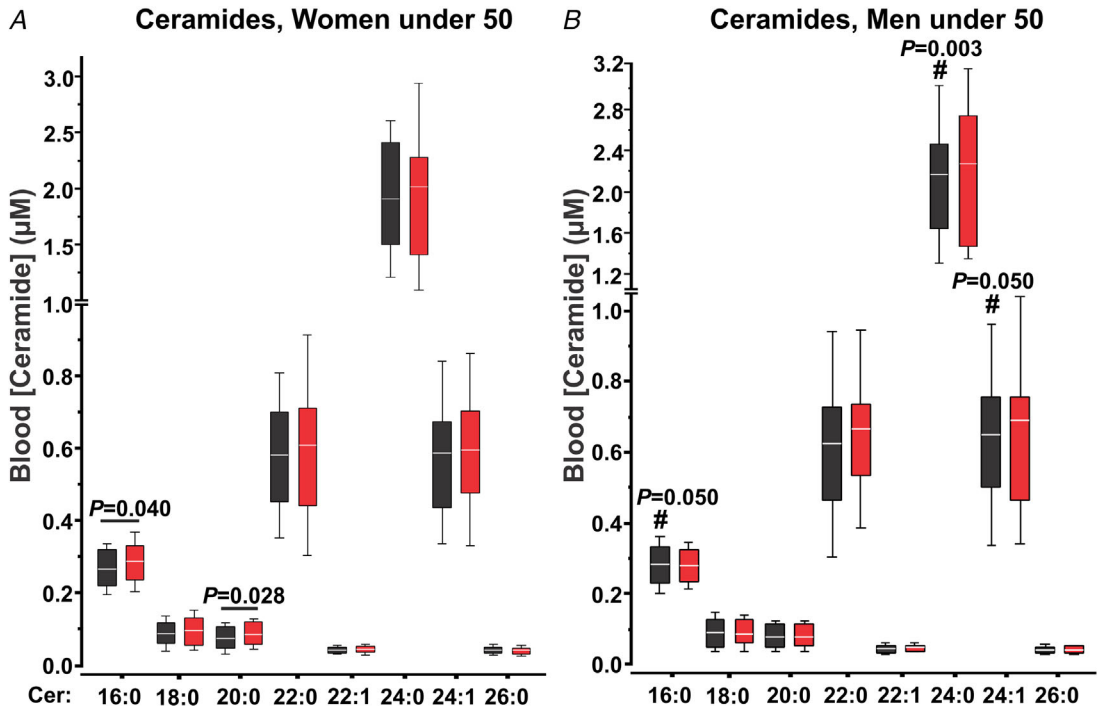

Figure 7. Blood ceramide levels in American adults <50 years of age, with and without hypertension
Absolute ceramide concentrations (micromolar) of women (*A*) and men (*B*) <50 years old. #Significance between sexes. Significance was determined via Welch's *t* test. Means (SD) are shown. Black or red bars indicate normo- or hypertensive groups, respectively; *n* = 60–200 human blood samples.

loading context, while excluding the additive neurohormonal/inflammatory effects.

Leveraging this new stretch protocol, we identified neutral sphingomyelinases (nSMase) as potent mechano-mediated regulators of cardiac caveolae, suggesting a possible pathological mediator of cardiac conditions when caveolae loss occurs and, conversely, when caveolae overexpression would be therapeutic (Markandeya et al., 2015; Patel et al., 2007). Prior to this study, there has been limited research on nSMase in the heart (Hernandez et al., 2000), with many studies using non-cardiac cell types, including but not limited to cultured skeletal myotubes (Moylan et al., 2014), mesenchymal stem cells (Makdissy et al., 2018) and various smooth muscle types (Czarny et al., 2003). In the present study, we found that not only is nSMase expressed in engineered and adult human cardiac tissue (Fig. 2*F*), but it might also have an active role in mediating

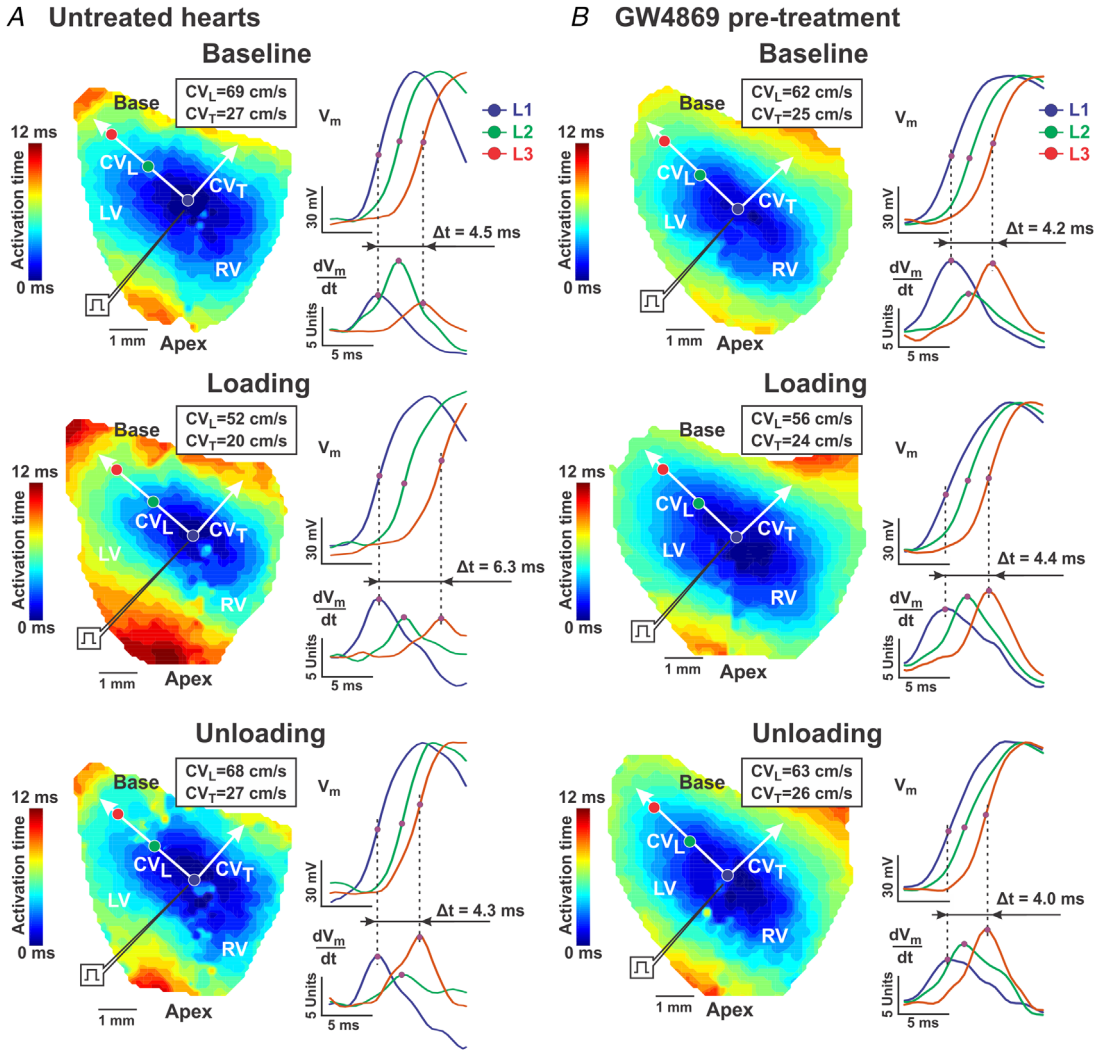

Figure 8. Effect of stretch on ventricular conduction measured by fluorescence optical mapping in isolated mouse left ventricles
Representative ventricular epicardial activation maps are shown for control hearts (*A*) and for hearts pretreated with GW4869 (30 min before loading; *B*) before loading (baseline), after 10 min of loading (30 mmHg) and after 20 min of unloading. Activation maps were reconstructed during constant electrical pacing (8 Hz). Epicardial pacing at the centre of the left ventricle produced an ellipsoidal spread of propagation, with fast conduction parallel to the fibre axis (longitudinal conduction) and slow conduction perpendicular to the fibre axis (transverse conduction). Arrows show the directions of conduction velocity measurements, longitudinal (CV_L) and transversal (CV_T). All the maps are plotted within the same time scale for comparison. The values of corresponding conduction velocities are presented at the right upper corner of each map. Near the maps, superimposed upstrokes of optical action potentials (V_m) and their derivatives (d*V*/d*t*) corresponding to recording sites in longitudinal direction (L1, L2 and L3 circles in corresponding maps) are shown. Time delays (Δt) are shown for each condition. Abbreviations: LV, left ventricle; RV, right ventricle.

the long-term effects of stretch on cardiac function. We showed that nSMase inhibition via GW4869 prevents stretch-induced reduction of caveolae-like structures (Fig. 1*F*) and mitigates the associated functional changes observed in stretched ECT (Fig. 3). As shown by Yu et al. (2005) in non-myocyte cells, we suspect that nSMase mechano-activation converts caveolar sphingomyelin to ceramide, which displaces cholesterol from caveolae, disrupting their formation. Although the difference in efficacy of GW4869 between nSMase types is unknown, GW4869 is likely to have a stronger inhibitory effect on sarcolemmal nSMase2 and nSMase3 (Moylan et al., 2014) than on the intracellular nSMase1, because GW4869 localizes to plasma membranes (Vuckovic et al., 2017). Furthermore, our RT-qPCR data demonstrate that nSMase3 (*SMPD4*) is the predominantly expressed caveolae-associated nSMase (Moylan et al., 2014) in adult human and mouse ventricles and human ECT (Fig. 2*F*), suggesting that nSMase3 is likely to be the main contributor to the observed nSMase-mediated effects. Given the suggested cardioprotective role of caveolae in the context of various cardiac conditions, such as hypertrophy (Markandeya et al., 2015), hypertension (Egorov et al., 2019), and heart failure (Wright et al., 2014), the identification of a mediator of caveolae loss provides an excellent drug target that could be used to mitigate the severity of these conditions. Previously, it has been postulated that the abundance of caveolae can be modulated only by altering the availability of cholesterol via methyl-β-cyclodextrin (Kozera et al., 2009) and caveolin (Galbiati et al., 2001) and cavin (Hill et al., 2008) scaffolding proteins using knockout or overexpression animal models. Our findings add a new dimension to caveolae regulation and highlight

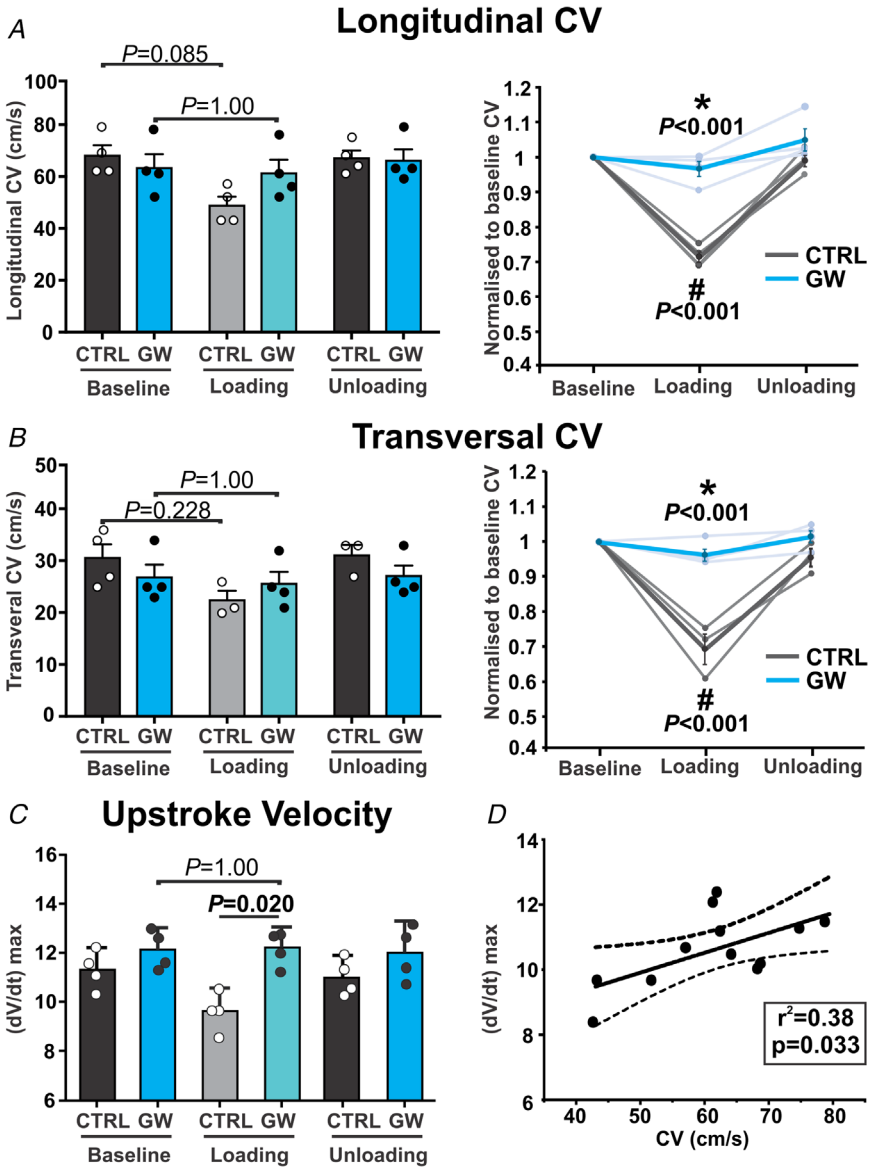

Figure 9. Acute stretch reduces ventricular conduction and upstroke velocity via neutral sphingomyelinase
A and *B*, mouse left ventricle longitudinal (*A*) and transversal (*B*) conduction velocity (CV), with normalization to baseline. *C* and *D*, maximal upstroke velocity (dV/dt_{max}; *C*) and correlation between CV and maximal upstroke velocity (*D*) of mouse left ventricles (non-GW4869 treated only). Groups: CTRL, no treatment control; GW, GW4869 pretreated. Significance was determined via two-way ANOVA with Bonferroni's *post hoc* test. *Significance between pretreatment (GW4869 *vs*. vehicle); #significance between pressure loading conditions. Means (SD) are shown, n = 3 or 4 mice per group.

nSMase as an upstream mechanoregulator of caveolar organization.

It is still not known whether nSMase is intrinsically mechanosensitive or mechano-activated, because various mechano-associated chemicals, such as angiotensin II (Bautista-Perez et al., 2015), TNF-α (Moylan et al., 2014) and ROS (Hernandez et al., 2000), might increase nSMase activity. Given the undetectable levels of *TNF-α* mRNA, it is unlikely that ECT nSMase is being activated by TNF-α protein, suggesting that nSMase is being activated only by mechanical cues in our experimental conditions. However, it has been shown that stretch mechano-activates NOX2 to produce ROS (Prosser et al., 2013), that ROS can activate nSMase (Hernandez et al., 2000) and that stretch increases ROS in our ECT medium (Fig. 2*C*). Therefore, it is possible that mechanically mediated activation of nSMase is augmented, at least in part, via ROS.

We also found that cyclic stretch induces production of ROS and short-chain ceramides in ECT medium and that GW4869 prevents the production of the latter (Fig. 2*A* and *C*). Although data provided by others suggest that stretch is a key component in the generation of ROS and ceramide (Czarny et al., 2003; Prosser et al., 2013), our findings extend these observations to indicate that in the cardiac context, nSMase might be a key mediator of stretch-mediated short-chain ceramide production. These results were supported indirectly by the human lipidomic data available from the MIDUS study, which enabled us to show that middle-aged and older adults with hypertension have significantly upregulated levels of specific ceramides in the systemic circulation (Figs 6 and 7).

Our contraction analyses strengthen the importance of caveolae in mediating β-adrenergic modulation of excitation–contraction coupling, implicating nSMase as a molecular mediator of stretch-induced blunting of the β-adrenergic response. We found that our stretched ECTs exhibit a blunted β-adrenergic contractile kinetic response, which was prevented by nSMase inhibition (Fig. 3*A* and *B*). In addition, this blunted response is most pronounced between 25 and 100% contraction (Fig. 3*F* and *G*), which might indicate that the caveolae disruption is interfering with proteins involved in excitation–contraction coupling rather than Ca^{2+} reuptake during the relaxation phase. Given the limited increase in fibrosis (Fig. 5*B*) and no changes in sarcomere length in our stretched ECT (Fig. 1*H*), we conclude that the effect is likely to be attributable to loss of caveolar structures via elevated nSMase activity, but we do not discount the possible additive role of fibrosis. However, our ECT stretch platform might not fully recapitulate animal models, because our ECT lack neurohormonal factors, such as angiotensin II, TNF-α and catecholamines, which might potentiate stretch-induced fibrosis.

The effect of mechanical stress on cardiomyocytes is well documented, with various groups demonstrating that increased mechanical stress, induced by increased pressure (Pfeiffer et al., 2014), swelling (Kozera et al., 2009; Turner et al., 2022) or physical stretch (Egorov et al., 2019; Khokhlova et al., 2022; MacDonald et al., 2020; Peyronnet et al., 2022), can disrupt cardiac conduction, induce apoptosis and arrhythmia, and alter cardiomyocyte tension and contraction. Supporting the relevance of nSMase in native tissue, our optical mapping experiments revealed that stretch-induced conduction velocity slowing is mediated by nSMase activation (Figs 8 and 9). However, the underlying molecular mechanism of stretch-induced conduction slowing remains unknown. Pfeiffer et al. (2014) found, in neonatal murine cardiomyocytes, that intact caveolae are required for stretch-induced conduction slowing. Stretch also increases intracellular ceramides (Huang et al., 2022; Shi et al., 2020), in addition to caveolae disruption (Markandeya et al., 2023) and alters membrane lipid composition (Boland & Drzewiecki, 2008), which could directly affect various ion channels involved in action potential propagation. For example, we found, in rat pulmonary vein myocardium, that stretch results in activation of the volume-sensitive, inward chloride current $I_{Cl,swell}$, leading to membrane resting potential depolarization and intra-vein conduction slowing (Egorov et al., 2019), probably via a depolarization-mediated decrease in availability of Na^+ channels. Furthermore, exogenous and endogenous ceramides elicit $I_{Cl,swell}$ in rabbit ventricular myocytes (Raucci et al., 2010), suggesting an nSMase-related mechanism. However, it is not known whether stretch-induced activation of $I_{Cl,swell}$ leads to resting membrane depolarization and conduction slowing in ventricular myocardium. Indeed, it has been shown that isolated ventricular myocytes have limited swelling-induced resting potential depolarization (by ∼3–5 mV) and only a negligible contribution of $I_{Cl,swell}$ to these changes (Ren et al., 2008). Importantly, ceramide can also reduce I_{Na} (Huang et al., 2022) and is involved in the activation of mechanosensitive cation (predominantly, Ca^{2+}) PIEZO1 channels (Shi et al., 2020), although stretch-induced ventricular conduction slowing has been found to be insensitive to the PIEZO1 inhibitor GsMTx-4 (Pfeiffer et al., 2014). In addition, Pfeiffer et al. (2014) showed a significant increase in sarcolemmal lipid density during stretch, suggesting the addition of material from subsarcolemmal caveolar stores to the sarcolemma, which could subsequently decrease the activity of Na^+ channels (Boland & Drzewiecki, 2008) and lead to conduction velocity slowing. Indeed, our analysis demonstrates reduced dV/dt_{max} in stretched hearts that is prevented by nSMase inhibition (Fig. 9*C*). Furthermore, we show that this decrease in dV/dt_{max} is significantly correlated with decreases in conduction velocity during

loading (Fig. 9*D*). These data suggest that mechanically mediated activation of nSMase in loaded mouse hearts might involve reduced I_{Na}, either by caveolae loss or by a direct action of ceramide on sodium channels. However, we also acknowledge the possible effect of stretch-induced nSMase activation on gap junctions and subsequent effects on conduction velocity. Upham et al. (2003) found, in non-cardiac cells, that membrane-permeable ceramides reduce gap junctional intercellular communication as measured by cell-to-cell dye transfer.

Overall, we have developed a new stretch protocol for inducing loss of caveolae-like structures in a human-based *in vitro* model that recapitulates the membrane morphology observed in spontaneously hypertensive rats and mice with transaortic constriction. This model induces a loss in β-adrenergic contractile kinetic response that is also observed during heart failure and hypertrophy induced by hypertension. We leveraged this ECT model and an acute volume overload mouse model to identify nSMase as a potent mediator in stretch-induced caveolae loss and reduced cardiac function attributable to mechanical stress.

Study limitations

Notwithstanding the importance and novelty of our findings, we acknowledge the limitations of the ECT stretch model owing to several factors, including the relative maturity of our differentiated iPSC myocytes, a relatively high baseline fibrosis compared with healthy human ventricular myocardium (Unverferth et al., 1986), the absence of resident immune cells, circulating inflammatory and neurohormonal factors, and the duration of the stretch protocol used. These factors might have contributed to the limited changes in both the percentage area fibrosis and fibrotic mRNA and the inability to detect mRNA for inflammatory cytokines (Fig. 5). For these reasons, our ECT stretch model might not fully recapitulate native cardiac hypertension or hypertrophy but can be used to test hypotheses regarding molecular mediators and processes related to chronically elevated stretch. Using this model, we were able to dissect specific mechanisms of nSMase mechanically mediated activation and factors that react to cardiac mechanical stress, but we recognize that owing to the presence of other inflammatory factors, including TNF-α (Moylan et al., 2014), we might expect that nSMase activation is elevated further in native hypertensive myocardium. Lastly, given that GW4869 is also a blocker of exosome generation, we acknowledge the possibility that prevention of paracrine signalling could play a role in the effects that we observed or other non-specific effects.

References

Atkins, F. L., Bing, O. H. L., Dimauro, P. G., Conrad, C. H., Robinson, K. G., & Brooks, W. W. (1995). Modulation of left and right ventricular beta-adrenergic receptors from spontaneously hypertensive rats with left ventricular hypertrophy and failure. *Hypertension*, **26**(1), 78–82.

Bautista-Pérez, R., Del Valle-Mondragón, L., Cano-Martínez, A., Pérez-Méndez, O., Escalante, B., & Franco, M. (2015). Involvement of neutral sphingomyelinase in the angiotensin II signaling pathway. *American Journal of Physiology-Renal Physiology*, **308**(10), F1178–F1187.

Berkowitz, L., Salazar, C., Ryff, C. D., Coe, C. L., & Rigotti, A. (2022). Serum sphingolipid profiling as a novel biomarker for metabolic syndrome characterization. *Frontiers in Cardiovascular Medicine*, **9**, 1092331.

Boland, L. M., & Drzewiecki, M. M. (2008). Polyunsaturated fatty acid modulation of voltage-gated ion channels. *Cell Biochemistry and Biophysics*, **52**(2), 59–84.

Böhm, M., Diet, F., Feiler, G., Kemkes, B., Kreuzer, E., Weinhold, C., & Erdmann, E. (1988). Subsensitivity of the failing human heart to isoprenaline and milrinone is related to beta-adrenoceptor downregulation. *Journal of Cardiovascular Pharmacology*, **12**(6), 726–732.

Calaghan, S., & White, E. (2006). Caveolae modulate excitation-contraction coupling and beta2-adrenergic signalling in adult rat ventricular myocytes. *Cardiovascular Research*, **69**(4), 816–824.

Chen, Y., Pat, B., Zheng, J., Cain, L., Powell, P., Shi, K., Sabri, A., Husain, A., & Dell'italia, L. J. (2010). Tumor necrosis factor-alpha produced in cardiomyocytes mediates a predominant myocardial inflammatory response to stretch in early volume overload. *Journal of Molecular and Cellular Cardiology*, **49**(1), 70–78.

Colligan, P. B., Relling, D. P., & Ren, J. (2002). Ceramide attenuates high glucose-induced cardiac contractile abnormalities in cultured adult rat ventricular myocytes. *Cellular and Molecular Biology*, **48**, OL251–OL257.

Czarny, M., Liu, J., Oh, P., & Schnitzer, J. E. (2003). Transient mechanoactivation of neutral sphingomyelinase in caveolae to generate ceramide. *Journal of Biological Chemistry*, **278**(7), 4424–4430.

De Lange, W. J., Farrell, E. T., Hernandez, J. J., Stempien, A., Kreitzer, C. R., Jacobs, D. R., Petty, D. L., Moss, R. L., Crone, W. C. & Ralphe, J. C. (2023). cMyBP-C ablation in human engineered cardiac tissue causes progressive Ca^{2+}-handling abnormalities. *Journal of General Physiology*, **155**(4), e202213204.

De Lange, W. J., Farrell, E. T., Kreitzer, C. R., Jacobs, D. R., Lang, D., Glukhov, A. V., & Ralphe, J. C. (2021). Human iPSC-engineered cardiac tissue platform faithfully models important cardiac physiology. *American Journal of Physiology-Heart and Circulatory Physiology*, **320**(4), H1670–H1686.

Díez, J. (2007). Mechanisms of cardiac fibrosis in hypertension. *Journal of Clinical Hypertension (Greenwich, Conn.)*, **9**(7), 546–550.

Egorov, Y. V., Lang, D., Tyan, L., Turner, D., Lim, E., Piro, Z. D., Hernandez, J. J., Lodin, R., Wang, R., Schmuck, E. G., Raval, A. N., Ralphe, C. J., Kamp, T. J., Rosenshtraukh, L V., & Glukhov, A V. (2019). Caveolae-mediated activation of mechanosensitive chloride channels in pulmonary veins triggers atrial arrhythmogenesis. *Journal of the American Heart Association*, **8**(20), e012748.

Galbiati, F., Engelman, J. A., Volonte, D., Zhang, X. L., Minetti, C., Li, M., Hou, H., Kneitz, B., Edelmann, W., & Lisanti, M. P. (2001). Caveolin-3 null mice show a loss of caveolae, changes in the microdomain distribution of the dystrophin-glycoprotein complex, and t-tubule abnormalities. *Journal of Biological Chemistry*, **276**(24), 21425–21433.

Gao, H.-L., Yu, X.-J., Hu, H.-B., Yang, Q.-W., Liu, K.-L., Chen, Y.-M., Zhang, Y., Zhang, D.-D., Tian, H., Zhu, G.-Q., Qi, J., & Kang, Y.-M. (2021). Apigenin improves hypertension and cardiac hypertrophy through modulating NADPH oxidase-dependent ROS generation and cytokines in hypothalamic paraventricular nucleus. *Cardiovascular Toxicology*, **21**(9), 721–736.

Glukhov, A. V., Fedorov, V. V., Kalish, P. W., Ravikumar, V. K., Lou, Q., Janks, D., Schuessler, R. B., Moazami, N., & Efimov, I. R. (2012). Conduction remodeling in human end-stage nonischemic left ventricular cardiomyopathy. *Circulation*, **125**(15), 1835–1847.

Glukhov, A. V., Flagg, T. P., Fedorov, V. V., Efimov, I. R., & Nichols, C. G. (2010). Differential K(ATP) channel pharmacology in intact mouse heart. *Journal of Molecular and Cellular Cardiology*, **48**(1), 152–160.

He, L., Kim, T., Long, Q., Liu, J., Wang, P., Zhou, Y., Ding, Y., Prasain, J., Wood, P. A., & Yang, Q. (2012). Carnitine palmitoyltransferase-1b deficiency aggravates pressure overload-induced cardiac hypertrophy caused by lipotoxicity. *Circulation*, **126**(14), 1705–1716.

Hernandez, O. M., Discher, D. J., Bishopric, N. H., & Webster, K. A. (2000). Rapid activation of neutral sphingomyelinase by hypoxia-reoxygenation of cardiac myocytes. *Circulation Research*, **86**(2), 198–204.

Hill, M. M., Bastiani, M., Luetterforst, R., Kirkham, M., Kirkham, A., Nixon, S. J., Walser, P., Abankwa, D., Oorschot, V. M. J., Martin, S., Hancock, J. F., & Parton, R. G. (2008). PTRF-Cavin, a conserved cytoplasmic protein required for caveola formation and function. *Cell*, **132**(1), 113–124.

Huang, S.-Y., Lu, Y.-Y., Lin, Y.-K., Chen, Y.-C., Chen, Y.-A., Chung, C.-C., Lin, W.-S., Chen, S.-A., & Chen, Y.-J. (2022). Ceramide modulates electrophysiological characteristics and oxidative stress of pulmonary vein cardiomyocytes. *European Journal of Clinical Investigation*, **52**(4), e13690.

Jensen, P. N., Fretts, A. M., Hoofnagle, A. N., Sitlani, C. M., Mcknight, B., King, I. B., Siscovick, D. S., Psaty, B M., Heckbert, S. R., Mozaffarian, D., Sotoodehnia, N., & Lemaitre, R. N. (2020). Plasma ceramides and sphingomyelins in relation to atrial fibrillation risk: The cardiovascular health study. *Journal of the American Heart Association*, **9**(4), e012853.

Ji, R., Akashi, H., Drosatos, K., Liao, X., Jiang, H., Kennel, P. J., Brunjes, D. L., Castillero, E., Zhang, X., Deng, L. Y., Homma, S., George, I. J., Takayama, H., Naka, Y., Goldberg, I. J., & Schulze, P. C. (2017). Increased de novo ceramide synthesis and accumulation in failing myocardium. *Journal of Clinical Investigation Insight*, **2**(14), e96203.

Jiang, G., Gong, H., Niu, Y., Yang, C., Wang, S., Chen, Z., Ye, Y., Zhou, N., Zhang, G., Ge, J., & Zou, Y. (2015). Identification of amino acid residues in angiotensin II type 1 receptor sensing mechanical stretch and function in cardiomyocyte hypertrophy. *Cellular Physiology and Biochemistry*, **37**(1), 105–116.

Kauhanen, D., Sysi-Aho, M., Koistinen, K. M., Laaksonen, R., Sinisalo, J., & Ekroos, K. (2016). Development and validation of a high-throughput LC-MS/MS assay for routine measurement of molecular ceramides. *Analytical and Bioanalytical Chemistry*, **408**(13), 3475–3483.

Khokhlova, A., Solovyova, O., Kohl, P., & Peyronnet, R. (2022). Single cardiomyocytes from papillary muscles show lower preload-dependent activation of force compared to cardiomyocytes from the left ventricular free wall. *Journal of Molecular and Cellular Cardiology*, **166**, 127–136.

Kozera, L., White, E., & Calaghan, S. (2009). Caveolae act as membrane reserves which limit mechanosensitive I(Cl,swell) channel activation during swelling in the rat ventricular myocyte. *PLoS ONE*, **4**(12), e8312.

Lian, X., Zhang, J., Azarin, S. M., Zhu, K., Hazeltine, L. B., Bao, X., Hsiao, C., Kamp, T. J., & Palecek, S. P. (2013). Directed cardiomyocyte differentiation from human pluripotent stem cells by modulating Wnt/β-catenin signaling under fully defined conditions. *Nature Protocols*, **8**(1), 162–175.

Lu, K., Seidel, T., Cao-Ehlker, X., Dorn, T., Batcha, A. M. N., Schneider, C. M., Semmler, M., Volk, T., Moretti, A., Dendorfer, A., & Tomasi, R. (2021). Progressive stretch enhances growth and maturation of 3D stem-cell-derived myocardium. *Theranostics*, **11**(13), 6138–6153.

Macdonald, E. A., Madl, J., Greiner, J., Ramadan, A. F., Wells, S. M., Torrente, A. G., Kohl, P., Rog-Zielinska, E. A., & Quinn, T. A. (2020). Sinoatrial node structure, mechanics, electrophysiology and the chronotropic response to stretch in rabbit and mouse. *Frontiers in Physiology*, **11**, 809.

Makdissy, N., Haddad, K., AlBacha, J. D., Chaker, D., Ismail, B., Azar, A., Oreibi, G., Ayoub, D., Achkar, I., Quilliot, D., & Fajloun, Z. (2018). Essential role of ATP6AP2 enrichment in caveolae/lipid raft microdomains for the induction of neuronal differentiation of stem cells. *Stem Cell Research & Therapy*, **9**(1), 132.

Markandeya, Y S., Gregorich, Z. R., Feng, L., Ramchandran, V., O' Hara, T., Vaidyanathan, R., Mansfield, C., Keefe, A. M., Beglinger, C. J., Best, J. M., Kalscheur, M. M., Lea, M. R., Hacker, T. A., Gorelik, J., Trayanova, N. A., Eckhardt, L. L., Makielski, J. C., Balijepalli, R. C., & Kamp, T. J. (2023). Caveolin-3 and Caveolae regulate ventricular repolarization. *Journal of Molecular and Cellular Cardiology*, **177**, 38–49.

Markandeya, Y S., Phelan, L J., Woon, M T., Keefe, A M., Reynolds, C R., August, B K., Hacker, T A., Roth, D M., Patel, H H., & Balijepalli, R C. (2015). Caveolin-3 overexpression attenuates cardiac hypertrophy via inhibition of T-type Ca^{2+} current modulated by protein kinase calpha in cardiomyocytes. *Journal of Biological Chemistry*, **290**(36), 22085–22100.

Moylan, J. S., Smith, J. D., Wolf Horrell, E. M., Mclean, J. B., Deevska, G. M., Bonnell, M. R., Nikolova-Karakashian, M. N., & Reid, M. B. (2014). Neutral sphingomyelinase-3 mediates TNF-stimulated oxidant activity in skeletal muscle. *Redox Biology*, **2**, 910–920.

Parton, R. G., & Del Pozo, M. A. (2013). Caveolae as plasma membrane sensors, protectors and organizers. *Nature Reviews Molecular Cell Biology*, **14**(2), 98–112.

Parton, R. G., Simons, K. (2007). The multiple faces of caveolae. *Nature Reviews Molecular Cell Biology*, **8**(3), 185–194.

Parton, R. G., Tillu, V. A., & Collins, B. M. (2018). Caveolae. *Current Biology*, **28**(8), R402–R405.

Patel, H. H., Tsutsumi, Y. M., Head, B. P., Niesman, I. R., Jennings, M., Horikawa, Y., Huang, D., Moreno, A. L., Patel, P. M., Insel, P. A., & Roth, D. M. (2007). Mechanisms of cardiac protection from ischemia/reperfusion injury: A role for caveolae and caveolin-1. *Federation of American Societies for Experimental Biology Journal*, **21**(7), 1565–1574.

Pavoine, C., & Pecker, F. (2009). Sphingomyelinases: Their regulation and roles in cardiovascular pathophysiology. *Cardiovascular Research*, **82**(2), 175–183.

Peyronnet, R., Desai, A., Edelmann, J.-C., Cameron, B. A., Emig, R., Kohl, P., & Dean, D. (2022). Simultaneous assessment of radial and axial myocyte mechanics by combining atomic force microscopy and carbon fibre techniques. *Philosophical Transactions of the Royal Society of London. Series B: Biological Sciences*, **377**(1864), 20210326.

Pfeiffer, E. R., Wright, A. T., Edwards, A. G., Stowe, J. C., McNall, K., Tan, J., Niesman, I., Patel, H. H., Roth, D. M., Omens, J. H., & McCulloch, A. D. (2014). Caveolae in ventricular myocytes are required for stretch-dependent conduction slowing. *Journal of Molecular and Cellular Cardiology*, **76**, 265–274.

Prosser, B. L., Ward, C. W., & Lederer, W. J. (2013). X-ROS signalling is enhanced and graded by cyclic cardiomyocyte stretch. *Cardiovascular Research*, **98**(2), 307–314.

Raucci, F. J., Wijesinghe, D. S., Chalfant, C. E., & Baumgarten, C. M. (2010). Exogenous and endogenous ceramides elicit volume-sensitive chloride current in ventricular myocytes. *Cardiovascular Research*, **86**(1), 55–62.

Ren, Z., Raucci, F. J., Browe, D. M., & Baumgarten, C. M. (2008). Regulation of swelling-activated Cl(-) current by angiotensin II signalling and NADPH oxidase in rabbit ventricle. *Cardiovascular Research*, **77**(1), 73–80.

Rodriguez-Cuenca, S., Barbarroja, N., & Vidal-Puig, A. (2015). Dihydroceramide desaturase 1, the gatekeeper of ceramide induced lipotoxicity. *Biochimica Et Biophysica Acta*, **1851**(1), 40–50.

Roth, G. A., Mensah, G. A., Johnson, C. O., Addolorato, G., Ammirati, E., Baddour, L. M., Barengo, N. C., Beaton, A. Z., Benjamin, E. J., Benziger, C. P., Bonny, A., Brauer, M., Brodmann, M., Cahill, T. J., Carapetis, J., Catapano, A. L., Chugh, S. S., Cooper, L. T., … Coresh, J., Group G-N-JGBoCDW. (2020). Global burden of cardiovascular diseases and risk factors, 1990–2019: Update from the GBD 2019 Study. *Journal of the American College of Cardiology*, **76**(25), 2982–3021.

Rybin, V O., Pak, E., Alcott, S., & Steinberg, S F. (2003). Developmental changes in beta2-adrenergic receptor signaling in ventricular myocytes: The role of Gi proteins and caveolae microdomains. *Molecular Pharmacology*, **63**(6), 1338–1348.

Shi, J., Hyman, A. J., De Vecchis, D., Chong, J., Lichtenstein, L., Futers, T. S., Rouahi, M., Salvayre, A. N., Auge, N., Kalli, A. C., & Beech, D. J. (2020). Sphingomyelinase disables inactivation in endogenous PIEZO1 channels. *Cell Reports*, **33**(1), 108225.

Turner, D. G. P., Tyan, L., Deguire, F. C., Medvedev, R Y., Stroebel, S. J., Lang, D., & Glukhov, A. V. (2022). Caveolin-3 prevents swelling-induced membrane damage via regulation of ICl,swell activity. *Biophysical Journal*, **121**(9), 1643–1659.

Ulmer, C. Z., Jones, C. M., Yost, R. A., Garrett, T. J., & Bowden, J. A. (2018). Optimization of Folch, Bligh-Dyer, and Matyash sample-to-extraction solvent ratios for human plasma-based lipidomics studies. *Analytica Chimica Acta*, **1037**, 351–357.

Unverferth, D. V., Baker, P. B., Swift, S. E., Chaffee, R., Fetters, J. K., Uretsky, B. F., Thompson, M. E., & Leier, C. V. (1986). Extent of myocardial fibrosis and cellular hypertrophy in dilated cardiomyopathy. *American Journal of Cardiology*, **57**(10), 816–820.

Upham, B. L., Koski, T. R., Rummel, A. M., Wilson, M. R., Horvath, A., & Trosko, J. E. (2003). Differential roles of 2, 6, and 8 carbon ceramides on the modulation of gap junctional communication and apoptosis during carcinogenesis. *Cancer Letters*, **191**(1), 27–34.

Vuckovic, S., Vandyke, K., Rickards, D. A., Mccauley Winter, P., Brown, S. H. J., Mitchell, T. W., Liu, J., Lu, J., Askenase, P. W., Yuriev, E., Capuano, B., Ramsland, P. A., Hill, G. R., Zannettino, A. C. W., & Hutchinson, A. T. (2017). The cationic small molecule GW4869 is cytotoxic to high phosphatidylserine-expressing myeloma cells. *British Journal of Haematology*, **177**(3), 423–440.

Wei, E. Q., Sinden, D. S., Mao, L., Zhang, H., Wang, C., & Pitt, G. S. (2017). Inducible Fgf13 ablation enhances caveolae-mediated cardioprotection during cardiac pressure overload. *Proceedings of the National Academy of Sciences*, **114**(20), E4010–E4019.

Wright, P. T., Nikolaev, V. O., O'hara, T., Diakonov, I., Bhargava, A., Tokar, S., Schobesberger, S., Shevchuk, A. I., Sikkel, M. B., Wilkinson, R., Trayanova, N. A., Lyon, A. R., Harding, S. E., & Gorelik, J. (2014). Caveolin-3 regulates compartmentation of cardiomyocyte beta2-adrenergic receptor-mediated cAMP signaling. *Journal of Molecular and Cellular Cardiology*, **67**, 38–48.

Wu, B. X., Clarke, C. J., Hannun, Y. A. (2010). Mammalian neutral sphingomyelinases: Regulation and roles in cell signaling responses. *Neuromolecular Medicine*, **12**(4), 320–330.

Wu, Q., Sun, L., Hu, X., Wang, X., Xu, F., Chen, B., Liang, X., Xia, J., Wang, P., Aibara, D., Zhang, S., Zeng, G., Yun, C., Yan, Y., Zhu, Y., Bustin, M., Gonzalez, F. J., & Jiang, C. (2021). Suppressing the intestinal farnesoid X receptor/sphingomyelin phosphodiesterase 3 axis decreases atherosclerosis. *Journal of Clinical Investigation*, **131**(9), e142865.

Yu, C., Alterman, M., & Dobrowsky, R. T. (2005). Ceramide displaces cholesterol from lipid rafts and decreases the association of the cholesterol binding protein caveolin-1. *Journal of Lipid Research*, **46**(8), 1678–1691.

Zhang, H., Huang, W., Liu, H., Zheng, Y., Liao, L. (2020). Mechanical stretching of pulmonary vein stimulates matrix metalloproteinase-9 and transforming growth factor-β1 through stretch-activated channel/MAPK pathways in pulmonary hypertension due to left heart disease model rats. *PLoS ONE*, **15**(9), e0235824.

Zhang, J., Klos, M., Wilson, G. F., Herman, A. M., Lian, X., Raval, K. K., Barron, M. R., Hou, L., Soerens, A. G., Yu, J., Palecek, S. P., Lyons, G. E., Thomson, J A., Herron, T. J., Jalife, J., & Kamp, T. J. (2012). Extracellular matrix promotes highly efficient cardiac differentiation of human pluripotent stem cells: the matrix sandwich method. *Circulation Research*, **111**(9), 1125–1136.

Zhang, J., Tao, R., Campbell, K. F., Carvalho, J. L., Ruiz, E. C., Kim, G. C., Schmuck, E. G., Raval, A. N., Da Rocha, A. M., Herron, T. J., Jalife, J., Thomson, J. A., & Kamp, T. J. (2019). Functional cardiac fibroblasts derived from human pluripotent stem cells via second heart field progenitors. *Nature Communications*, **10**(1), 2238.

Additional information

Data availability statement

The datasets generated during and/or analysed during the present study are available from the corresponding author on reasonable request, with the exception of human ceramide data, for which permission must be obtained through MIDUS.

Competing interests

The authors declare no conflicts of interest.

Author contributions

D.G.P.T. designed the study, collected significant portions of data, analysed all data, wrote the majority of the manuscript, and generated figures. W.J.D.D. collected and assisted in E.C.T. contraction data analysis and writing. Y.Z. and Y.G. collected and assisted in analysis and writing of mass spectrometry data. C.L.C. and J.S. assisted in human ceramide data collection, analysis, and writing. T.J.K. and J.C.R. made significant contributions to the design of the study and writing of the manuscript. A.V.G. assisted in optical mapping data collection and analysis and made major contributions to the writing of the manuscript, figure generation, and study design. All authors approved the final version of the manuscript and agree to be accountable for all aspects of the work in ensuring that questions related to the accuracy or integrity of any part of the work are appropriately investigated and resolved. All persons designated as authors qualify for authorship, and all those who qualify for authorship are listed.

Funding

This work was supported by grants from National Institutes of Health (R01HL141214, R01HL139738 and R01HL146652), American Heart Association Career Development Award (16SDG29120011) and the Wisconsin Partnership Program (4140) to A.V.G. D.G.P.T. would like to acknowledge a National Institutes of Health Predoctoral Training grant (T32GM008688), support provided by the University of Wisconsin-Madison Office of the Vice Chancellor for Research and Graduate Education with funding from the Wisconsin Alumni Research Foundation, and an American Heart Association Predoctoral Fellowship (903203). Y.G. would like to acknowledge National Institutes of Health (R01 GM125085, R01 HL096971, GM117058 and S10 OD018475). The MIDUS project was supported by awards from the National Institute on Aging (P01 AG030166 and U19AG051426).

Acknowledgements

The author(s) thank the UW-Madison Translational Research Initiatives in Pathology laboratory (TRIP), supported by the UW Department of Pathology and Laboratory Medicine, UWCCC (P30 CA014520) and the Office of The Director-NIH (S10 OD023526) for use of its facilities and services. Finally, the authors thank Randall J. Massey and the SMPH Electron Microscopy Facility (UW-Madison) for critical assistance in preparing and imaging ECTs, and Janay Walters for manuscript editing and suggestions.

Keywords

caveolae, ceramide, hypertension, neutral sphingomyelinase, stretch, tissue engineering

Supporting information

Additional supporting information can be found online in the Supporting Information section at the end of the HTML view of the article. Supporting information files available:

Peer Review History